Chemical Geology 593 (2022) 120758

Contents lists available at ScienceDirect

Chemical Geology

journal homepage: www.elsevier.com/locate/chemgeo

Mapping intrashell variation in Mg/Ca of brachiopods to external growth lines: Mg enrichment corresponds to seasonal growth slowdown

Tamás Müller [a,b,*], Adam Tomašových [c], Matthias López Correa [d,e], Regina Mertz-Kraus [f], Tomáš Mikuš [g]

[a] ELTE Eötvös Loránd University, Institute of Geography and Earth Sciences, Department of Geology, Budapest, Hungary
[b] Isotope Climatology and Environmental Research Centre, Institute for Nuclear Research, Bem tér 18/C, H-4026 Debrecen, Hungary
[c] Earth Science Institute, Slovak Academy of Sciences, Dúbravska cesta 9, 84005 Bratislava, Slovakia
[d] Consiglio Nazionale delle Ricerche, Istituto di Scienze Marine, Via Gobetti 101, 40129 Bologna, Italy
[e] GeoZentrum Nordbayern, Universität Erlangen-Nürnberg, Loewenichstrasse 28, 91054 Erlangen, Germany
[f] Institut für Geowissenschaften, Johannes Gutenberg-Universität Mainz, J.-J.-Becher-Weg 21, D-55128 Mainz, Germany
[g] Earth Science Institute, Slovak Academy of Sciences, Ďumbierska 1, 974 11, Banska Bystrica, Slovakia

ARTICLE INFO

Keywords:
Brachiopoda
Biomineralization
Mg/Ca ratio
S/Ca ratio
Sr/Ca ratio
Growth rate
Seasonality

ABSTRACT

Determining secular changes in seawater temperature and Mg/Ca ratio is of high importance in paleooceanographic, paleoenvironmental and paleoecological studies. On the one hand, intra-shell variation in Mg/Ca in brachiopod shells is used to reconstruct historical changes in temperature and in seasonality. On the other hand, intra-shell analyses show a weak relationship between Mg/Ca and $\delta^{18}O$, but a positive correlation between Mg/Ca and Sr/Ca, and an increase of Mg/Ca at growth lines, indicating that Mg/Ca does not simply track seawater temperature alone. Internal growth lines are rarely visible in brachiopod shells, and the relation between growth lines that mark growth slowdown or cessation and Mg/Ca fluctuation is thus not properly understood. Here, using four species of extant brachiopods from the NE Pacific and the SW Pacific, from environments with low seasonality in seawater temperature (<5 °C), and two species of Late Triassic brachiopods (Western Carpathians), we measure intra-shell ontogenetic variation in Mg/Ca, S/Ca and Sr/Ca with laser ablation ICP-MS and electron microprobe. In contrast to previous studies, we map variation in Mg, S, and Sr to external growth lines. We find that, first, zones of Mg/Ca enrichment in the secondary layer form 10–50 μm-thick discrete bands or clusters of micrometric bands that consistently terminate at major external, predominantly annual growth lines that are associated with distinct notches that correspond to mantle retractions in most species. These bands generate distinct peaks in Mg/Ca that stand above low, more uniformly distributed background Mg/Ca values along laser-ablation and microprobe transects. The magnitude of Mg/Ca in these bands is comparable to Mg/Ca in the primary layer, exceeding background values of Mg/Ca in the secondary layer by 5–20 mmol/mol (by a factor of two to five). Second, Mg enrichment in discrete bands is closely associated with an increase in S concentrations in the secondary layer. Therefore, even when Mg and S uptake is expected to be highest under fast precipitation rate, these empirical observations show that Mg and S enrichment occur in the zones that were precipitated at times of a significant growth reduction (e.g., in cold-temperate brachiopods studied here during winters when primary productivity is low). The mechanisms for this paradox are unclear but can be related to uptake of Mg by amorphous calcium carbonate (ACC) to delay the transformation of ACC to calcite during the formation of growth lines. Therefore, intra-shell variation in Mg/Ca in brachiopods with major growth lines is primarily determined by seasonal decline or cessation in shell growth and not by seasonal changes in seawater temperature.

* Corresponding author at: Department of Geology, Eötvös Loránd University, Pázmány Péter promenade 1/C, Budapest H-1117, Hungary.
E-mail address: beregond02@gmail.com (T. Müller).

https://doi.org/10.1016/j.chemgeo.2022.120758
Received 18 February 2021; Received in revised form 27 January 2022; Accepted 1 February 2022
Available online 5 February 2022

1. Introduction

Rhynchonelliformean brachiopods represent a reliable geochemical archive because they secrete low magnesium calcite that is resistant to diagenetic alteration (Lowenstam, 1961; Veizer et al., 1999; Brand et al., 2003; Ullmann and Korte, 2015), they were abundant in a broad range of marine environments during the Phanerozoic (Novack-Gottshall and Lanier, 2008; Zhang et al., 2015), and the secondary layer of brachiopod shell tends to be in isotopic equilibrium with the ambient seawater (Carpenter and Lohmann, 1995; Parkinson et al., 2005; Brand et al., 2013). Brachiopods secrete their shells as they precipitate an outer primary layer with acicular calcite and an inner secondary layer that forms calcite fibers, secreted by the outer mantle epithelium (Williams, 1968; Roda et al., 2019a, 2019b). Although oxygen isotopes in brachiopod shells are used in estimates of past climate, seawater temperature, and seasonality (Popp et al., 1986; Grossman et al., 1993; Brand et al., 2013; Suan et al., 2010; Yamamoto et al., 2010; Price et al., 2013; Kocsis et al., 2020), such inferences remain difficult due to uncertainties in estimates of seawater isotopic composition. Therefore, additional independent proxies such as elemental concentrations or clumped isotopes are needed to estimate seawater temperature (Henkes et al., 2013; Bajnai et al., 2018). Alternatively, Mg/Ca and Sr/Ca in marine biogenic carbonates can provide information on seawater temperature because Mg and Sr tends to show a higher partitioning rate in the function of temperature in the calcitic shell of marine calcifiers (e.g. Buening and Carlson, 1992; Carpenter and Lohmann, 1992; Beck et al., 1992; Rosenthal et al., 1997; Lea et al., 1999; Anand et al., 2003; Ries, 2010; Schöne et al., 2011), and furthermore, the element ratios can track changes in ocean chemistry as well (e.g. Dickson, 2002; Ries, 2004; Ullmann et al., 2013).

Although element incorporation in biotic calcite or aragonite does not occur at thermodynamic equilibrium, taxon-specific paleotemperature estimates were calibrated for foraminifers (Lear et al., 2000; Martin et al., 2002; Barker et al., 2005), corals (Watanabe et al., 2001), bivalves (Klein et al., 1996; Steuber and Rauch, 2005; Poulain et al., 2015), belemnites (Nunn and Price, 2010) and brachiopods (Butler et al., 2015). Secular changes in seawater Mg/Ca complicate the relationship between Mg/Ca of calcite and seawater temperature in the fossil record, especially at times with low seawater Mg/Ca, as during the Mesozoic Era (Immenhauser et al., 2005). However, residence times of Mg and Ca in seawater are on the scale of 13 and 1 Myr, respectively (Broecker and Yu, 2011). Therefore, intra-shell variability in Mg/Ca and/or among-shell comparisons of Mg/Ca performed at high stratigraphic resolution can be used to infer seawater temperature and climatic variability not confounded by variability in seawater Mg/Ca (Grossman et al., 1996; Powell et al., 2009). However, the application of Mg/Ca ratios to assess past seawater temperature on the basis of brachiopod shells remains poorly understood, owing to the physiological effects and owing to the confounding role of precipitation rate that may affect incorporation of Mg into calcitic shells (Berner, 1975; Carpenter and Lohmann, 1992; Davis et al., 2000; Ullmann and Pogge von Strandmann, 2017; Jurikova et al., 2020). For instance, inorganic calcite precipitation experiments show that an increasing precipitation rate favors Mg incorporation into the crystal lattice (Mavromatis et al., 2013). However, other mechanisms such as slower dehydration of Mg relative to Ca during inorganic precipitation and also the Mg/Ca ratio of the experimental fluid could also affect, but in an opposite way, the Mg incorporation into the calcite as the function of precipitation rate (Gabitov et al., 2014). In contrast, laboratory experiments indicate that bands distinctly enriched in Mg/Ca form at times when shell growth and calcite precipitation almost ceased, indicating differences between Mg incorporation under inorganic and biologically-controlled precipitation (Jurikova et al., 2020). Rollion-Bard et al. (2019) suggested that the Mg-enrichment can be in fact related to uptake by amorphous calcium carbonate (a presumed precursor of calcite in the primary and secondary layer of brachiopod shells), rather than to uptake by calcite.

On the one hand, temperature sensitivity of Mg/Ca was supported by intraspecific analyses that showed that Mg/Ca positively correlates with seawater temperature (Pérez-Huerta et al., 2008; Butler et al., 2015; Clark et al., 2016; Rollion-Bard et al., 2019) and by interspecific analyses that documented that $MgCO_3$ negatively correlates with $\delta^{18}O$ (Brand et al., 2013). On the other hand, however, intra-shell analyses demonstrated that $\delta^{18}O$ and Mg/Ca in fact do not correlate within the secondary layer of several terebratulids (Ullmann et al., 2017a), in contrast to relatively high correlations that were documented in calcitic bivalves (Vander Putten et al., 2000). Furthermore, Mg/Ca of the secondary layer tends to correlate moderately positive with Sr/Ca (Armendáriz et al., 2008; Ullmann et al., 2017a; Jurikova et al., 2020), whereas the temperature dependence of Mg/Ca and Sr/Ca predicted by thermodynamic effects should generate inverse correlations. Finally, Mg/Ca of the secondary layer correlates strongly with S/Ca (Mii and Grossman, 1994; Grossman et al., 1996; Cusack et al., 2007; Cusack et al., 2008a), and Mg and S concentrations in brachiopod shells can be enhanced by the presence of these elements in organic matter (England et al., 2007; the contribution of organics thus need to be carefully accounted for in the analyses of Mg/Ca, Schöne et al., 2010). However, Cusack et al. (2008b) showed that Mg enrichment is not associated with the organic components, and Richardson et al. (2019) showed that sulfur in brachiopod shells predominantly relates to the calcite material and has a negligible concentration in the organic matrix.

The potential of brachiopod shells to reveal average (annual) seawater temperature or seasonal variability in seawater temperature on the basis of Mg/Ca thus remains unclear. This lack of understanding is probably caused by the lack or rarity of explicit analyses linking growth increments and growth lines with Mg/Ca variation (Buening and Carlson, 1992; Gaspard et al., 2018). Although brachiopod growth lines tend to be visible as major external growth interruptions on their surface, the orientation of internal growth increments within the secondary layer is difficult to reconstruct (Hiller, 1988; Tomašových and Farkaš, 2005) Therefore, Mg/Ca wiggles observed in LA-ICP-MS or EPMA transects (Powell et al., 2009; Butler et al., 2015; Clark et al., 2016) cannot be easily mapped to external growth lines in brachiopods.

Here, using laser ablation inductively coupled plasma mass spectrometry (LA-ICP-MS) and electron microprobe analyses (EPMA), we (i) explicitly link the location of external growth lines with Mg/Ca variability in element maps in extinct and extant individuals of both impunctate (rhynchonellid) and punctate (terebratulid) brachiopods, (ii) assess co-variation between Mg, Sr, and S, and (iii) evaluate whether intra-shell variation in Mg/Ca can be linked (1) to seawater temperature changes (Pérez-Huerta et al., 2008), (2) to ontogenetic changes in growth rate that are unrelated to changes in seawater temperature (predicting that longitudinal transects parallel with growth should show a significant decline in Mg/Ca; Buening and Carlson, 1992), or (3) to intra-annual changes in the shell growth rate (Jurikova et al., 2020). We use both laser-ablation and microprobe to validate the difference between these methods in their spatial resolution (35 μm in laser ablation versus 8 μm in microprobe) and image resolution (higher resolution of back-scattered electrons allows better tracking shell structures) generate congruent results, especially when the thickness of bands enriched with Mg can be just 10 μm. We demonstrate that the maxima in Mg/Ca ratios detected in growth transects closely coincide with the location of major external growth lines, and postulate that intra-shell Mg/Ca ratio variability is thus associated with seasonal growth cessation rather than by seasonal changes in seawater temperature.

2. Materials and methods

2.1. Extant brachiopods

Element ratios (Mg/Ca, S/Ca, Sr/Ca) and the location of external growth lines were analyzed in four extant brachiopod species, including one rhynchonellid with impunctate structure and three terebratulids

with punctate structure. In total, two specimens of *Terebratalia transversa* (TT07 and TT09), two specimens of *Magasella sanguinea* (DS04 and DS05), two specimens of *Notosaria nigricans* (DS07 and DS08), and one specimen of *Laqueus erythraeus* (LA) were analyzed by LA-ICP-MS and one specimen of each species was analyzed by EPMA.

T. transversa and *L. erythraeus* were collected at two locations in the NE Pacific (San Juan Islands and southern California) and *M. sanguinea* and *N. nigricans* were collected at one location in the SW Pacific (New Zealand), all characterized by a moderate range in seasonal seawater temperature (less than 5–6 °C). *T. transversa* was sampled in August 2002 at Point George at 25 m water depth (TT09 - dorsal valve length = 29.5 mm, 48.5564 N, −122.987 W) and in August 2006 at Mosquito Pass at 15 m water depth (locality 1 in Tomašových, 2008, 48.5871 N, −123.17 W) (TT07–30.5 mm) (Fig. 1A). Bathymetric gradient in seawater temperature is extremely mild at San Juan Islands owing to strong mixing of waters, with differences between 0 and 75 m that are less than 1 °C. The mean seawater temperature is ~9 °C (with annual range of mean monthly seawater temperature between 7 and 13 °C at Mosquito Pass and between 7 and 11 °C at Point George). The salinity is between 29 and 30 psu at both locations.

The terebratulid *Magasella sanguinea* (DS04 dorsal valve length = 35 mm, DS05 = 31.5 mm) and the rhynchonellid *N. nigricans* (DS07 dorsal valve length = 18 mm, DS08 = 16.5 mm) were collected at 20 m water depth in the Doubtful Sound in New Zealand (Fig. 1B) in February 2010 by Alan Logan. Doubtful Sound is indented into the SW coast of South Island, it is 2 km wide, and has a 40 km-long main channel, with two openings to the Tasman Sea (Lamare and Stewart, 1998). The fjord is characterized by a thin, low-salinity surface layer throughout the fiord (5–10 psu). Instrumental data show mean seawater temperature of 13 °C (with an annual range of mean monthly seawater temperature between 12 and 17 °C) and a mean salinity of 34 psu (Fig. 1).

The terebratulid *Laqueus erythraeus* (LA) was collected in the southern California Bight of the San Pedro shelf (Fig. 1C) at 116 m water depth (33.5648 N, −118.1461 W) during a monitoring survey in 1994 (station 1476, Stull et al., 1999), with annual mean seawater temperature equal to 10 °C, and annual range of mean monthly seawater temperature between 9 and 11 °C, and salinity equal to 33.5 psu. The San Juan Island Archipelago and the Doubtful Sound are located in cool-temperate provinces, whereas the southern California Bight is located in a warm-temperate province (Spalding et al., 2007).

For an overview of the above described information see Table 1.

2.2. Extinct brachiopods

To assess whether the intra-shell variability in element ratios can be also detected in fossil brachiopods, we use EPMA on two brachiopod species from the Upper Triassic (Rhaetian) Tethyan deposits. The impunctate rhynchonellid *Fissirhynchia fissicostata* was collected from marly limestones of the Hybe Formation (lithologically and environmentally comparable to the Eiberg Member of the Kössen Formation in the Eastern Alps) at Hybe section (Michalík, 1973). They were deposited in mid-shelf environments close to the storm wave base (Hronic Unit, Western Carpathians). The punctate terebratulid *Rhaetina gregaria* was collected from marly limestones of the Fatra Formation (comparable to the Hochalm Member of the Kössen Formation) deposited in shallower, inner-shelf environments above the storm wave base (Fatric Unit, Western Carpathians) at Bystrý potok section (Tomašových, 2004).

2.3. Material preparation

Ventral valves were measured in all analyses of extant and extinct brachiopods. The shells were embedded in epoxy resin and cut in two halves along the symmetry axis to generate longitudinal sections capturing ontogenetic changes in the concentrations of elements. Ventral valves were oriented so that sections pass through the beak and the pedicle foramen and run towards the anteriormost margin (similarly as in Buening and Carlson, 1992). One half was used to generate polished slabs that were analyzed with LA-ICP-MS (seven specimens of extant species: DS07, DS08, DS04, DS05, TT07, TT09, and LA) and another half was used for preparation of polished and carbon coated thin-sections that were analyzed with EPMA (four extant specimens: DS07, DS04, TT09, and LA; and two fossil specimens: *F. fissicostata* and *R. gregaria*). Both fossil brachiopods possess minor concentrations of Mn (< 250 ppm) and sufficiently high Sr (> 400 ppm) (determined by EPMA measurement) to confirm an excellent preservation of calcitic fibers in their secondary shell layer (Korte et al., 2005), and the thin, Mg-enriched bands are not enriched or depleted in these two elements relative to other portions of the secondary shell layer of fossil brachiopods (Fig. 12C-D).

2.4. LA-ICP-MS analyses

LA-ICP-MS analyses were performed at the Institut für Geowissenschaften, Johannes Gutenberg Universität Mainz, using an ESI NWR 193 excimer laser ablation system coupled to an Agilent 7500ce

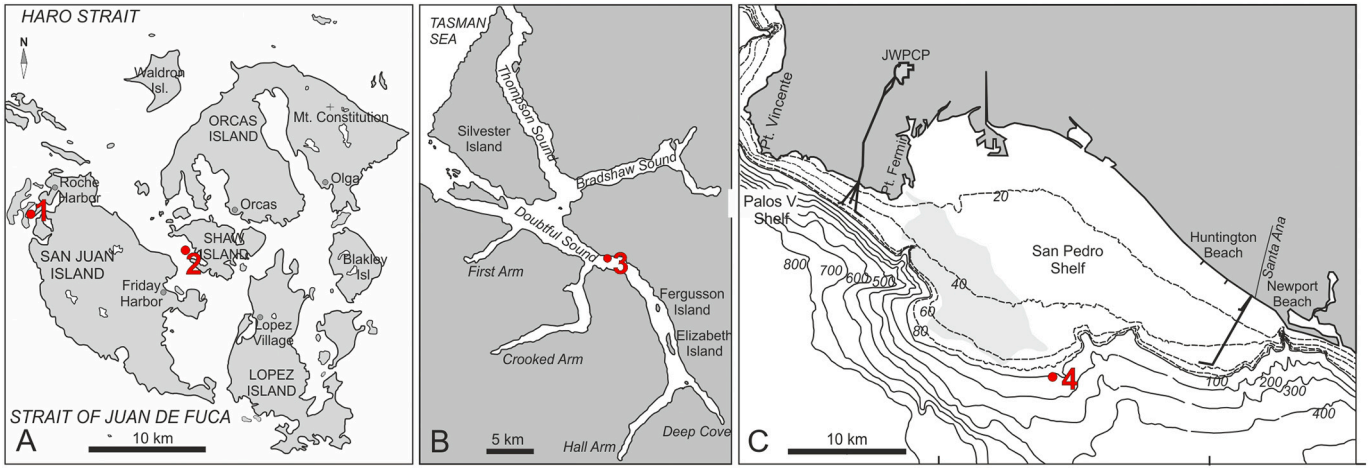

Fig. 1. Geographic locations of sites in the San Juan Channel and Mosquito Pass (A, San Juan Islands) (*Terebratalia transversa* at location 1 – Mosquito Pass, location 2 – George Point off Shaw Island), in the Doubtful Sound in New Zealand (B, *Magasella sanguinea* and *Notosaria nigricans* at location 3), and in the southern California Bight (C, *Laqueus erythraeus* at location 4) where extant brachiopods were collected. The maps were digitized on the basis of standard Google maps (http://maps.google.com/).

Table 1
Summarized information regarding the origin and environment of extant brachiopod samples.

Species (specimen)	Location	Date of collection	Water depth	Annual mean seawater T	Annual range of seawater T	Salinity
Terebratalia transversa (TT09)	San Juan Island, Point George, WA, USA, 48.5564 N, −122.987 W	August 2002	25 m	9 °C	7–11 °C	29–30 psu
T. transversa (TT07)	San Juan Island, Mosquito Pass, WA, USA, 48.5871 N, −123.17 W	August 2006	15 m	9 °C	7–13 °C	29–30 psu
Magasella sanguinea (DS04 and DS05)	Doubtful Sound, New Zealand	February 2010 (by Alan Logan)	20 m	13 °C	12–17 °C	34 psu
Notosaria nigricans (DS07 and DS08)	Doubtful Sound, New Zealand	February 2010 (by Alan Logan)	21 m	13 °C	12–17 °C	34 psu
Laqueus erythraeu (LA)	San Pedro shelf, CA, USA, 33.5648 N, −118.1461 W	1994	116 m	10 °C	9–11 °C	33.5 psu

Quadrupole ICP-MS instrument to determine trace element concentrations. After pre-ablation, data were acquired by line scans using a beam diameter of 35 μm and a scan speed equal to 15 μm/s at a pulse repetition rate of 10 Hz and an energy density of ~3 J/cm^2. For each analysis, background signals were measured for 20 s. The multi-element synthetic glass NIST SRM 610 was used for calibration of the element concentrations, applying the preferred values for NIST SRM 610 reported in the GeoReM database (http://georem.mpch-mainz.gwdg.de/; Application version 21, January 2017) (Jochum et al., 2005, 2011) as the "true" concentrations, to calculate the element concentrations of the samples. Monitored isotopes included ^{25}Mg, ^{43}Ca, ^{44}Ca, ^{55}Mn, and ^{88}Sr. ^{43}Ca was used for internal standardization. Mg/Ca ratio in mmol/mol was computed with Ca^{2+} values of 390,000 μg/g (i.e., this concentration corresponds to average concentrations of Ca in these brachiopods on the basis of EPMA). Data processing included a background correction and was performed following the methods of Longerich et al. (1996). Individual measurements were averaged over 50 μm in all analyses of longitudinal transects, and over 20 μm in all analyses of vertical transects. Standards were measured before and after the analyses of each transect (all data are available in the Appendix A and B) and show a high level of reproducibility, with <5% relative standard deviation (RSD) for Mg/Ca, and < 3% RSD for Sr/Ca. These uncertainties are shown as error bar intervals in Figs. 5–8. Detection limits are mostly less than 0.5 μg/g for the measured elements.

LA-ICP-MS transects were oriented in two ways. First, one or two longitudinal transects were made through the secondary layer in each specimen of four extant species (one transect close to the inner surface and one transect close to the outer surface), spanning 20–40 mm in total length, running parallel with the direction of ontogenetic growth trajectory from the beak towards the anteriormost margin, covering the whole ontogenetic growth of each specimen. This transect is expected to detect both ontogenetic and seasonal variability affecting the precipitation of the secondary layer. Second, a vertical transect penetrating through the primary and the secondary layer (typically less than 1–2 mm in length), starting on the external surface and terminating on the internal surface, was measured on each slab. Although measurement spots were adjusted so that punctae were not measured, some punctae along the line transects were not fully avoided during these analyses because the beam diameter was larger (35 μm) than the general width of punctae (~8–20 μm) and the resolution of camera images did not always allow the detection of punctal boundaries.

2.5. Electron probe micro-analyses

2–3 mm-long EPMA transects and EPMA maps were taken in the secondary layer in the anterior parts of valves with conspicuous external growth lines that form overhangs (Fig. 2). Transects were oriented so that they maximized the direction parallel with the growth starting from the external surface and running anteriorward at a relatively low angle, thus being similar to longitudinal transects, but also crossing the primary layer (Fig. 2). The step size between individual measurements was 25 μm in extant specimens and in *R. gregaria* and 50 μm in *F. fissicostata*. Two EPMA transects were taken on the specimens *T. transversa* and *N. nigricans*, each ~1 mm away from each other (Fig. 2). The punctae were avoided in EPMA analyses.

Electron probe micro-analyses (EPMA) in wavelength-dispersive

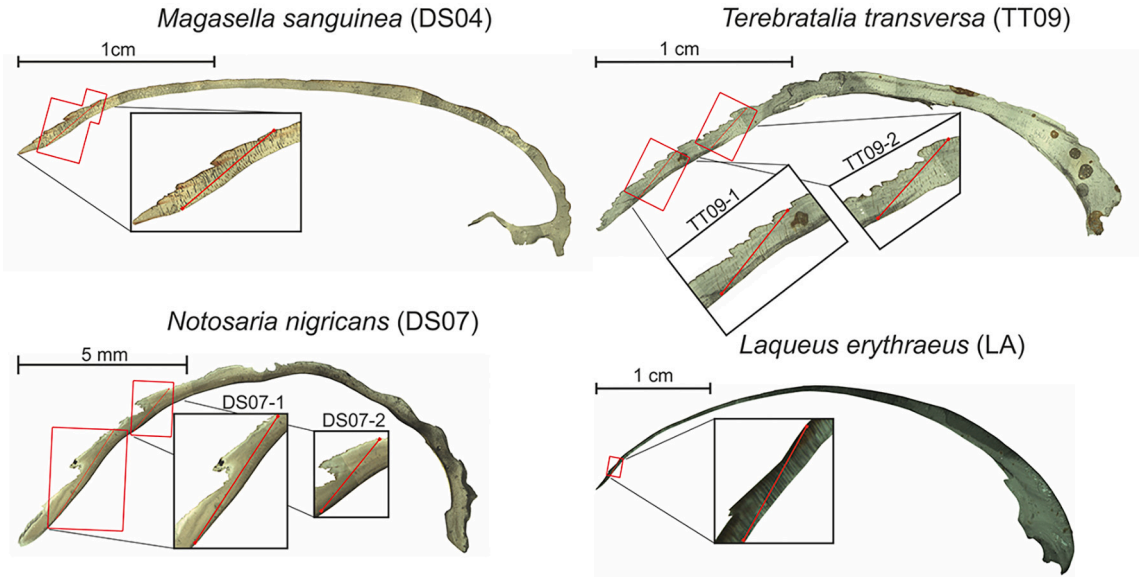

Fig. 2. Microscope images of the thin-sections of the selected specimens of four extant species and locations (anterior) of EPMA sections and mapped areas.

spectrometry (WDS) mode and mapping mode were performed using JEOL JXA 8530FE equipment at the Earth Sciences Institute in Banská Bystrica (all data are available in the Appendix C). An accelerating voltage of 15 kV and 16 nA probe current were used. The typical spot beam diameter was 8 μm for analyses and 1 μm for mapping. The EPMA was calibrated using natural and synthetic reference materials. Counting time: 20 s on peak, 10 s on background. Used reference materials, X-ray lines and detection limit (D.L.) in μg/g is calculated as follows: Ca (Kα, 31–33) – diopside, Mg (Kα, 42–48) – diopside, Sr (Lα, 64–86) – celestite, S (Kα, 26–31) – barite. The detection limit is calculated in μg/g follows:

$$\text{D.L.} = \frac{1}{\frac{InetSTD}{mass(\%)STD}} \sqrt{\frac{2\ x\ Iback}{tback}}$$

where

I_{back}: Average intensity of background X-rays.

t_{back}: Counting time of the background signals.

I_{netSTD}: Intensity of net X-rays of the reference material.

mass $(\%)_{STD}$: Mass concentration in the reference material.

Raw counts were converted to wt% of oxides using ZAF matrix correction factors (where Z: atomic number correction; A: absorption correction; F: characteristic fluorescence correction). For elemental mapping following conditions were used: accelerating voltage 15 kV, probe current 15 nA, beam diameter 1 μm, dwell time 60 msec and resolution 1190 × 858 pixels. Uncertainties computed as two standard errors below and above the measured values were added to the figures.

2.6. Matching external growth lines to Mg/Ca fluctuations

To assess whether the external growth lines correspond to boundaries between annual increments, first, we measured the distances between individual well-visible external growth lines and the posteriormost margin along the ventral valve midline (thus corresponding to ventral valve lengths at time of growth line formation) in three extant species (external growth lines were not well-visible on L. *erythraeus*). The growth line is defined as a notch or an indentation visible in a longitudinal cross-section of valves, forming an abrupt deviation of the external valve surface from the growth curvature (Fig. 3). Second, to quantify the age-dependent rate of growth, the ontogenetic successions of ventral valve lengths (terminating at individual growth lines, and thus achieved at a given ontogenetic age) were fitted to the corresponding ontogenetic age with von Bertalanffy growth models with the package fishmethods (Nelson, 2014) (Fig. 4). These models estimate three parameters, including (1) the asymptotic length, (2) the growth parameter (*K*) that determines how quickly organisms achieve their asymptotic length, and (3) the initial length parameter that determines the length at the onset of growth. Third, growth rate estimated with this method were compared with independent growth-rate estimates of three species (*T. transversa, M. sanguinea*, and *N. nigricans,* Thayer, 1977; Ostrow, 2004; Lee et al., 2011). The alignment of internal growth lines (i.e., an angle at which external growth lines pass through the valves) is uncertain in brachiopod sections. Therefore, the matching of growth lines observed on the external surface with Mg/Ca fluctuations measured at some distance from the external surface in LA-ICP-MS transects is difficult. However, this matching can be explicitly documented in EPMA transects that are coupled with well-resolved back-scattered electron images and in EPMA maps.

3. Results

3.1. External growth lines and growth rate

Specimens of *T. transversa*, *N. nigricans*, and *M. sanguinea* (collected at depths <25 m) show well-visible external growth lines, locally forming overhangs or steps that indicate a marked mantle regression associated with growth slowdown or cessation (comparable to growth lines formed by inward reflection of the mantle edge as documented by Hiller, 1988) (Fig. 3). External growth lines also form clusters of three-four lines spaced across 1–2 mm in *T. transversa* (Fig. 3A-B). In contrast, external growth lines in L. *erythraeus* (collected at 116 m) are weak. The spacing of external growth lines declines with ontogenetic age in *T. transversa*, *N. nigricans*, and *M. sanguinea* towards the anterior margin where growth lines are clustered, being separated by ~1 cm in the posterior portions and by few mm in the anterior portions (Fig. 4). Nine major external lines were counted in both specimens of *N. nigricans* and *M. sanguinea*. Seven to eight clusters of densely-spaced growth lines, separated by valve portions without growth lines, were counted in two specimens of *T. transversa*, respectively. Three lines of evidence indicate that the major external growth lines (or closely-spaced clusters of lines in *T. transversa*) in cold-temperate brachiopods from the San Juan

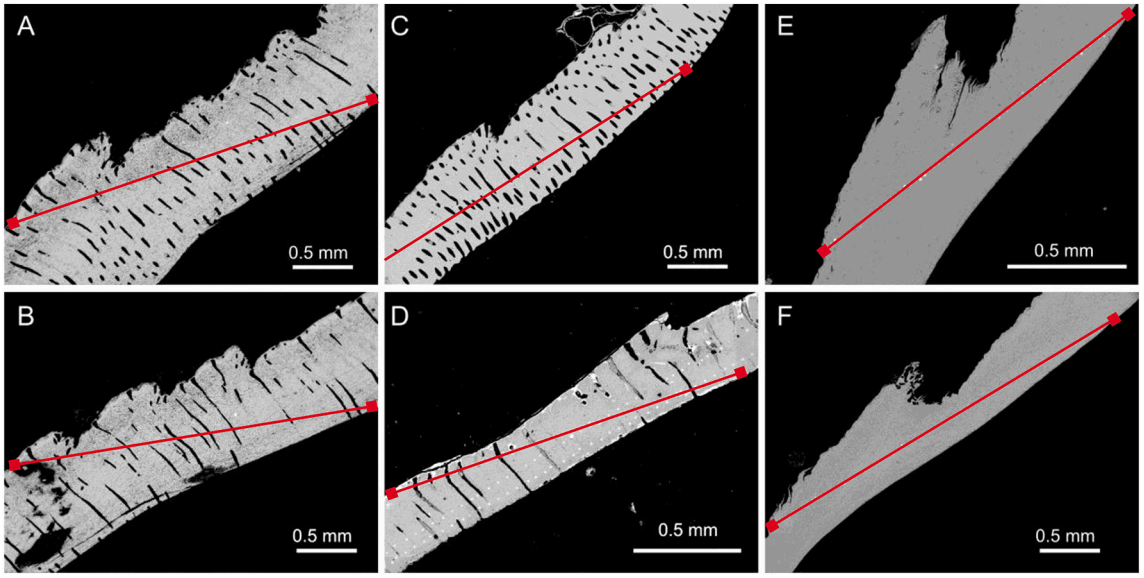

Fig. 3. Back-scattered electron images showing the location of external growth lines that are visible as major overhangs in cross-sections of *T. transversa* (A- TT09–2; B- TT09–1), *M. sanguinea* (C), *L. erythraeus* (D), and *N. nigricans* (E –DS07–2; F –DS07–1). Red lines are marking the tracks of EPMA transects. (For interpretation of the references to color in this figure legend, the reader is referred to the web version of this article.)

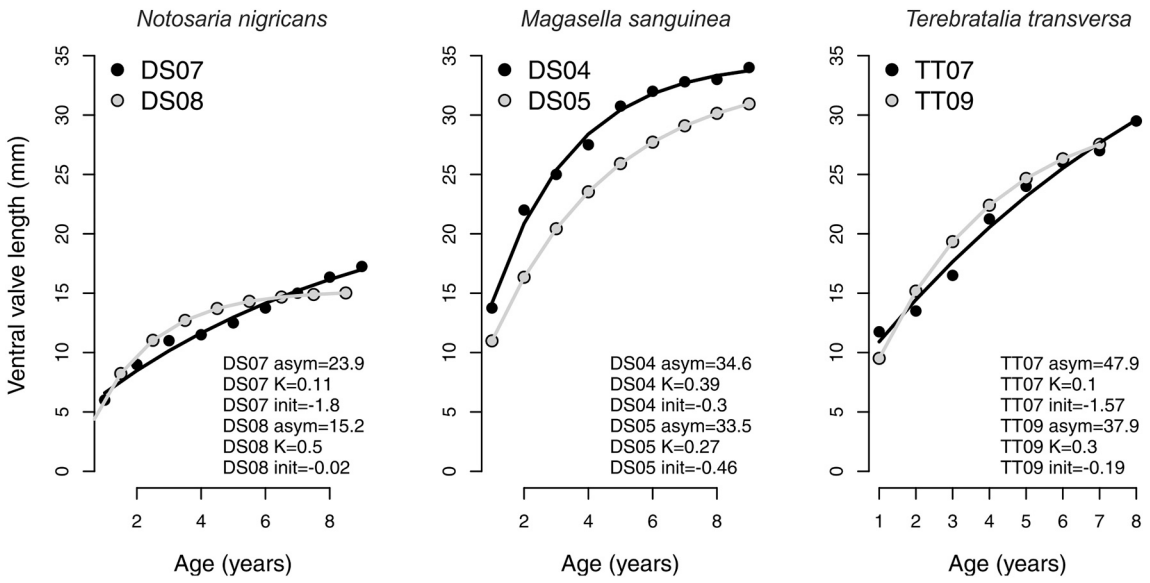

Fig. 4. Growth curves showing the fits of the von Bertalanffy growth models in three extant brachiopod species (each represented by two specimens), with ages assigned on the basis of major external growth lines that coincide with internal Mg/Ca maxima. They show that growth rate declined through ontogeny, with the exception of one specimen of TT07 where the fit indicates that the growth did not decline after the first year of growth.

Archipelago and New Zealand represent annual increments, with nine lines in both individuals of *N. nigricans* and in both individuals of *M. sanguinea* and with 7–8 lines in two individuals of *T. transversa*. First, the spacing of external growth lines in *T. transversa, N. nigricans* and *M. sanguinea* is in accordance with the expected decline in growth rate with increasing ontogenetic age. Growth curves fitted by von Bertalanffy growth model (see Brey et al., 1995) show that growth rate declined through ontogeny, with the exception of one specimen of TT07 where the fit indicates that growth rate did not decline after the first year of growth (Fig. 4). Second, assuming that external growth lines have annual frequency, growth rates are congruent with previously published estimates of growth rates in *T. transversa*, *N. nigricans*, and *M. sanguinea* (Thayer, 1977; Ostrow, 2004; Lee et al., 2011). The growth rate in *T. transversa* declined from 10 to 11 mm/y in the first year to 6–7 mm/y in the second and third year, and to 3–4 mm/y during the later years (slightly higher or similar to *T. transversa* growth rates documented by Thayer, 1977). Growth rate in *M. sanguinea* declined from 11 to 14 mm/y in the first years to 7–8 mm/y in the third year, and to 3–4 mm/y during the later years (comparable to growth rates of *M. sanguinea* from outer parts of the Doubtful Sound documented by Ostrow, 2004). Growth rate in *N. nigricans* declined from 4 to 6 mm/y in the first two years to 3–4 mm/y in the third and fourth year, and to 1–2 mm/y during the later years (comparable to growth rates of *M. sanguinea* in Lee et al., 2011 who observed that *N. nigricans* grew 2–5 mm/year over the first three years).

3.2. Mg/Ca and Sr/Ca variability in LA-ICP-MS transects

Vertical and longitudinal LA-ICP-MS profiles show three major patterns. First, the primary intra-shell variation in Mg/Ca in extant specimens, as observed also in other studies (i.e. Pérez-Huerta et al., 2008), is related to the difference between the primary layer (10–30 mmol/mol) and the secondary layer (3–20 mmol/mol) that can be observed in vertical transects (Fig. 5). However, vertical transects show that Mg/Ca is highly variable within the primary layer and (Griesshaber et al., 2007 also showed that Mg content in the primary layer was even smaller than in the secondary layer in some brachiopod specimens) and within the secondary layer. The difference in Mg/Ca between the primary and the secondary layer is not observed in *Magasella sanguinea* individuals. One source of intra-shell variation is related to the location of muscle scars and internal shell structures, with significant enrichment in Mg at locations penetrating through median septum in the specimen DS04 (Fig. 5; other sections did not pass through similar structures). However, strong fluctuations in Mg/Ca, approaching values observed in the primary layer, occur also within the secondary layer without any septal or muscle structures.

Second, longitudinal transects through the secondary layer of whole valves show that Mg/Ca ratios do not show any major or consistent trends and on average remain remarkably constant in all four species (Figs. 6–8). In *T. transversa*, the slope of the relation between the ontogenetic stage (approximated by distance of the measurement from the posterior margin, i.e., smaller distance means younger ontogenetic age) and Mg/Ca (measured in mmol/mol per mm) is either insignificant in TT7 (slope $= -0.008$, $p = 0.49$) or positive in TT9 (slope $= 0.11$, $p < 0.0001$). In *N. nigricans*, the slope of the relation between the ontogenetic stage and Mg/Ca is either insignificant in DS7 (slope $= 0.02$, $p = 0.41$) or negative in DS8 (slope $= -0.07$, $p = 0.0037$). In *M. sanguinea*, the slope of the relation between the ontogenetic stage and Mg/Ca is either weakly positive in DS4 (slope $= 0.026$, $p = 0.0003$) or weakly negative in DS5 (slope $= -0.02$, $p = 0.009$). These results differ from previous studies that suggested that Mg/Ca declines with age (and thus reducing growth rate) in terebratulid brachiopods (Buening and Carlson, 1992).

Third, longitudinal transects through the secondary layer capture strong fluctuations in Mg/Ca (Figs. 6–8), with sharp and relatively narrow peaks in Mg/Ca that are less than 0.5 mm thick in *N. nigricans* and *M. sanguinea* and are clustered in ~1–2 mm-zones in *T. transversa*. These maxima in Mg/Ca attain 20 mmol/mol in *T. transversa*, 10–15 mmol/mol in *N. nigricans*, 10 mmol/mol in *M. sanguinea*, and 10 mmol/mol in L. *erythraeus*. These values are comparable to those observed in the primary layer. The maxima in the secondary layer are separated by smaller and more uniformly distributed or mildly fluctuating Mg/Ca values (i.e., background Mg/Ca values). This basic alternation of narrow maxima with broader minima is also visible within short vertical transects in anterior parts of valves (Fig. 5). *T. transversa*, *N. nigricans* and *M. sanguinea* possess well-developed external growth lines that spatially coincide with sharp maxima in Mg/Ca (see vertical lines associated with numbers in Figs. 6–8). The magnitude of these sharp maxima is stronger in outer than in inner transects in *T. transversa* and *M. sanguinea*, whereas the background minima tend to show similar Mg/Ca values in

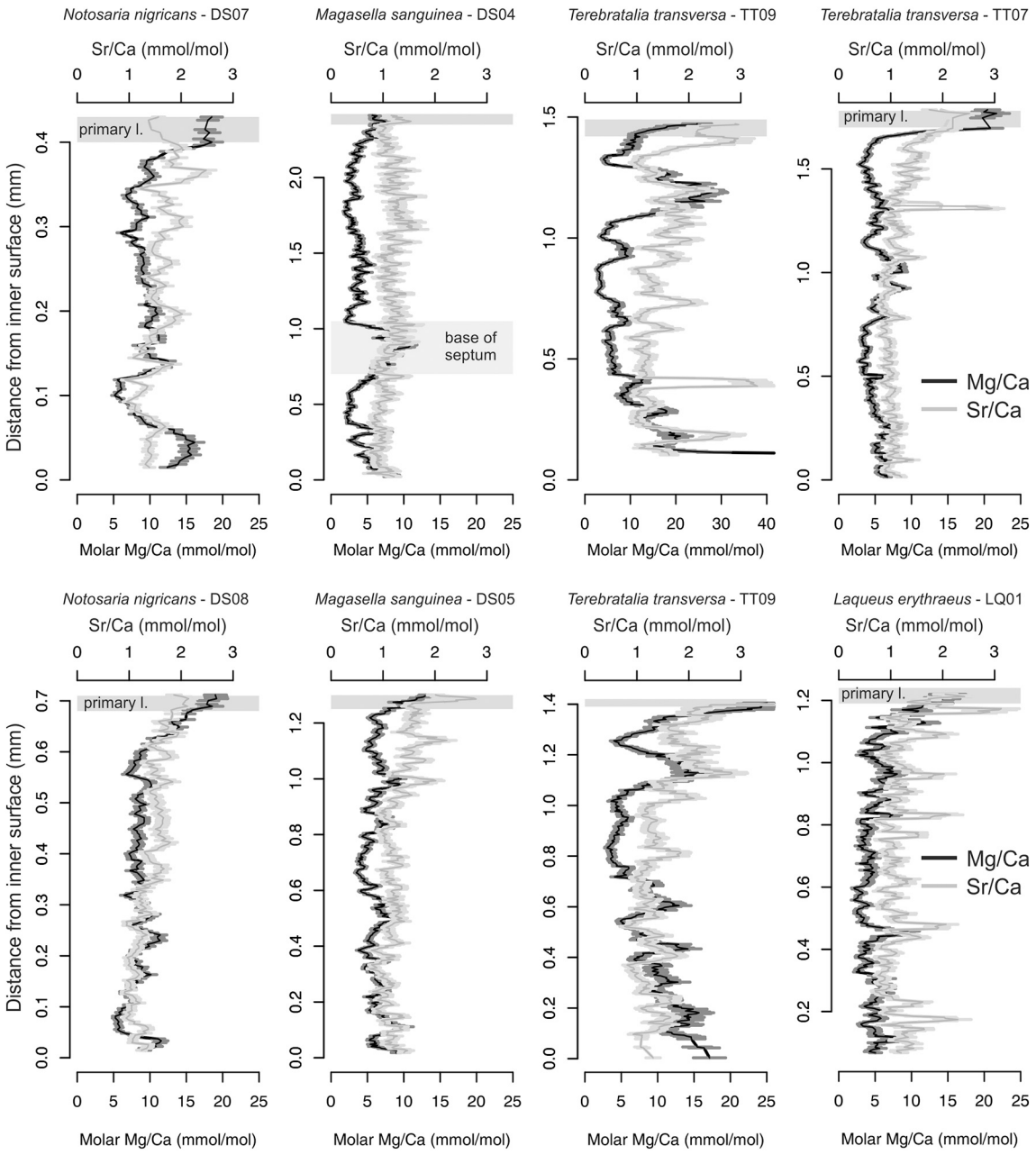

Fig. 5. Vertical LA-ICP-MS transects capturing variation in Mg/Ca (black lines) and Sr/Ca (gray lines) between the innermost (bottom) and external surface (top), with the primary layer in the uppermost part. Dark-gray band is the primary layer. Septum in DS04 is a calcitic ridge formed by secondary shell layer that extends above the internal valve surface. With the exception of DS04, the base of vertical transects coincides with the internal valve surface. Error bars were computed on the basis of relative standard deviation estimated from the analysis of reference materials. With the exception of *T. transversa* TT09 where the top figure shows the middle part and the bottom figure captures the anterior part of the valve, all profiles were located in the middle part of valves. In DS04, two closely-positioned transects pass through median septum, that is ~1 mm thick.

inner and outer transects. In the outer transect in TT9, there is a one-to-one correspondence between the clusters of external growth lines (gray vertical bands) and Mg/Ca peaks. This correspondence becomes less straightforward in the inner transect in the posterior part of the valve as the magnitude of Mg/Ca peaks becomes smaller. Several peaks in Mg/Ca also coincide with the location of external growth lines and can be correlated between the inner and outer transects in TT07.

Similarly, as Mg/Ca, Sr/Ca values do not show any major trend in longitudinal transects (Figs. 6–8). Sr/Ca depends on the ontogenetic stage positively but rather weakly in TT07 (slope = 0.009, $p < 0.0001$), in TT09 (slope = 0.011, $p < 0.0001$), in DS07 (slope = 0.009, $p < 0.0001$), in DS08 (slope = 0.005, $p = 0.07$), in DS04 (slope = 0.007, $p < 0.0001$), and in DS05 (slope = 0.002, $p = 0.005$). The Spearman rank correlations between Sr/Ca and Mg/Ca are weakly positive or insignificant (Supplementary Fig. 1, r [DS07] = 0.21, $p = 0.001$, r [DS08] = 0.16, $p = 0.007$, r [DS04] = 0.47, $p < 0.001$, r [DS05] = −0.01, $p = 0.78$, r [inner TT07] = 0.07, $p = 0.15$, r [outer TT07] = 0.11, $p = 0.007$, r [inner TT09] = 0.6, $p < 0.001$, [outer TT09] = 0.21, $p = 0.15$, r [LA] = 0.17, $p < 0.001$).

3.3. Mg/Ca, S/Ca and Sr/Ca variability in EPMA WDS transects and in maps

In *T. transversa*, Mg/Ca values range between 3.8 and 30.3 mmol/

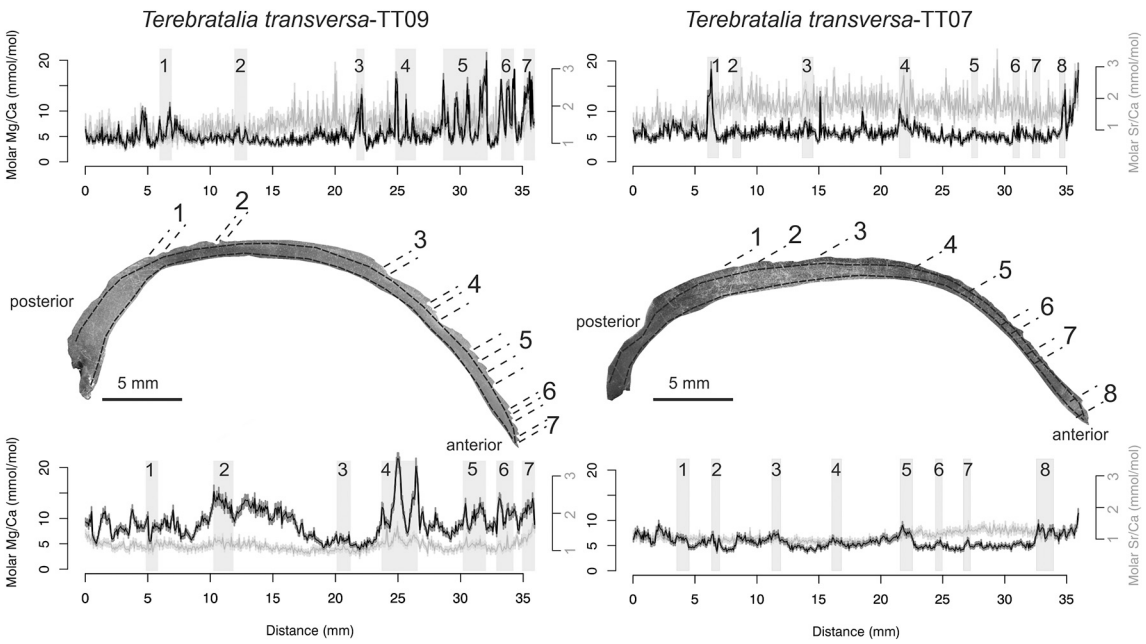

Fig. 6. LA-ICP-MS profiles showing variations in Mg/Ca (black lines) and Sr/Ca (gray lines) in outer (top row) and inner transects (bottom row) of two specimens of *Terebratalia transversa* collected off San Juan Islands (specimen TT9 collected at Point George, with the outer transect TT9–01 and the inner transect TT9–02) and specimen TT7 in Mosquito Pass, with the outer transect TT7–01 and the inner transect TT7–02). The location of external growth lines (forming clusters of lines in the anterior parts of TT9) is shown in vertical gray lines and numbered. The outer and inner longitudinal transects are represented by black dashed lines. Error bars were computed on the basis of relative standard deviation estimated from the analysis of reference materials.

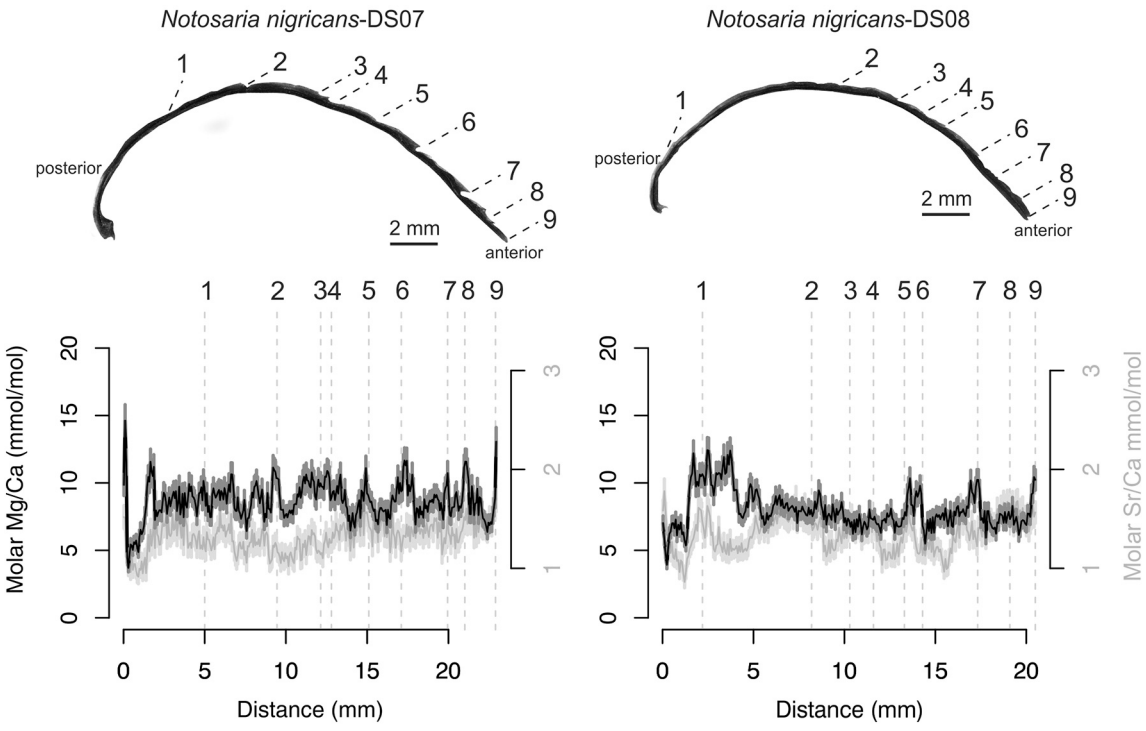

Fig. 7. LA-ICP-MS profiles showing variation in Mg/Ca (black lines) and Sr/Ca (gray lines) in inner transects of two specimens of the rhynchonellid brachiopod *Notosaria nigricans* collected in the Doubtful Sound (collected alive at the same location). Mg/Ca maxima closely match the expected location of nine external growth lines (vertical dashed lines). Error bars were computed on the basis of relative standard deviation estimated from the measurements of reference materials.

mol in the section located in the anterior valve portions (transect TT09–1 in Fig. 11A). Several narrow WDS peaks in Mg/Ca terminate at external growth lines, with a sharp increase from low values between growth lines (~5 mmol/mol) to ~10–20 mmol/mol in narrow bands that terminate at external growth lines. A similar pattern can be observed in the anteriormost portions (transect TT09–2 Fig. 11B), Mg/Ca values vary between 3.8 and 25.3 mmol/mol, also displaying distinct narrow WDS peaks separated by broader lows. Each of the WDS peaks can be linked to Mg-enriched bands on the EPMA maps and to external growth lines. In *N. nigricans* (Fig. 11C-D), Mg/Ca values range between 6

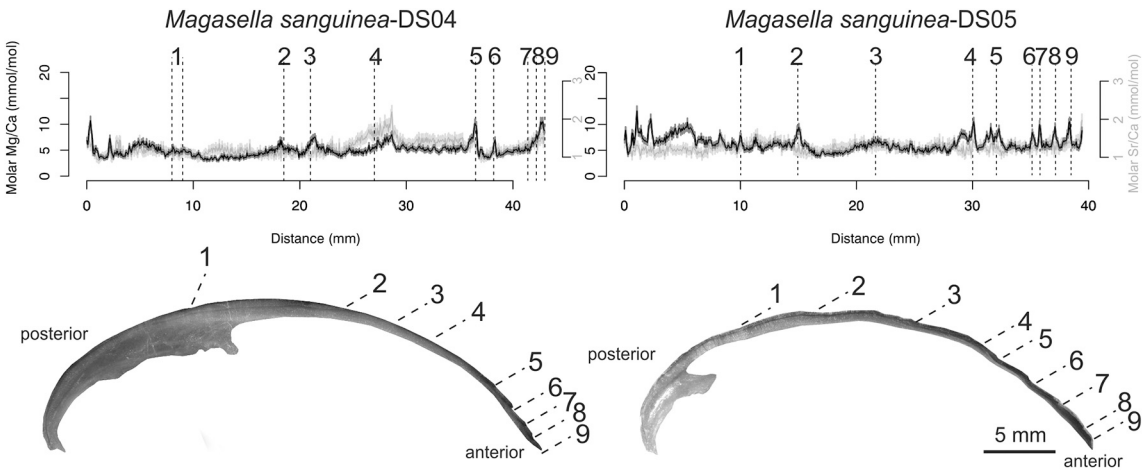

Fig. 8. LA-ICP-MS profiles showing variation in Mg/Ca (black lines) and Sr/Ca (gray lines) in outer longitudinal transects of two specimens of the terebratulid brachiopod *Magasella sanguinea* collected in the Doubtful Sound (collected alive at the same location). Mg/Ca maxima in outer transects closely match the position of nine external growth lines (vertical dashed lines). Error bars were computed on the basis of relative standard deviation estimated from the measurements of reference materials.

and 17 mmol/mol in the section DS07–1 and between 6 and 22.1 mmol/mol in the section DS07–2 (Fig. 11), where the highest values correspond to the primary layer. In *M. sanguinea* (Fig. 12A), five narrow Mg/Ca peaks (10–18 mmol/mol) occur in the secondary layer of the shell, where they correspond to thin bands in the maps that terminate at external growth lines. Within these bands, Mg/Ca abruptly increases by 6–10 mmol/mol relative to low values (Fig. 12A), and a sixth peak in Mg/Ca located at the outermost part of the shell is related to the Mg enrichment in the primary layer. *L. erythraeus* (section LA) shows Mg/Ca values between 4.4 and 12.4 mmol/mol (Fig. 12B). *F. fissicostata* (Fig. 12D) shows similar fluctuations in Mg/Ca as observed in *M. sanguinea* and *T. transversa*, with Mg/Ca ranging between 3.8 and 21.4 mmol/mol (Figs. 11 and 12). Several peaks, corresponding to bright bands in elemental maps, are visible where Mg/Ca values increase by ~10–15 mmol/mol. The terebratulid *R. gregaria* shows Mg/Ca values ranging between 7.2 and 21.5 mmol/mol (Fig. 12C), with four distinct peaks in Mg/Ca. The S/Ca EPMA transects show patterns that are closely aligned with patterns in Mg/Ca. S/Ca values range between 1 and 18.2 mmol/mol, with high ratios limited to the narrow micrometric bands also enriched in Mg, and low ratios being typical of the rest of valves (Fig. 12). In the *M. sanguinea* (DS04) the average S/Ca ratio is 5.36 mmol/mol, but in the growth bands it can reach ~8–18 mmol/mol. The two sections DS07–1 and DS07–2 of the species *N. nigricans* exhibit a similar range of S/Ca ratio with an average of 3.2 mmol/mol and an increase within the growth bands up to 5–8 mmol/mol. Mean values in the section, TT09–1 and TT09–2 of *T. transversa* are 4 and 4.7 mmol/mol while within the area of the growth bands values increase to 8–15 mmol/mol. L. *erythraeus* (LA) provided a mean S/Ca ratio of 5.3 mmol/mol and peak values ~7–10 mmol/mol. In one of the fossil specimens, *R. gregaria* S/Ca averages to 4.9 mmol/mol while in growth bands values increase to 6–8.4 mmol/mol. *F. fissicostata* provided mean value of S/Ca of 2.8 mmol/mol and in peaks values reach 4–6.8 mmol/mol. The peaks in S/Ca thus invariably overlap with the peaks in Mg/Ca. Sr/Ca values do not track these peaks in Mg/Ca and S/Ca (Fig. 12).

To conclude Mg/Ca values along EPMA transects (Figs. 11 and 12) form sharp and narrow peaks in all specimens, similarly as observed in LA-ICP-MS transects (Figs. 6–8). In addition to the Mg enrichment in the primary layer detected by LA-ICP-MS, EMPA element maps of *T. transversa* and *M. sanguinea* show discrete, 10–50 μm-thick bands within the secondary layer, where Mg concentration is notably higher than in the surrounding regions in all specimens (Figs. 11 and 12). These Mg-enriched bands are also visible in *N. nigricans* and L. *erythraeus*, but their visibility becomes weaker towards the internal valve surface (Figs. 11 and 12). Similar bands enriched in Mg are also clearly visible in *R. gregaria* and *F. fissicostata*. Element maps reveal that S shows a remarkably similar distribution as Mg, i.e., S is significantly enriched in the micrometric bands (by a factor of two to five), in contrast to lower values characteristic for the secondary shell layer as typically observed in present-day brachiopods with EPMA (England et al., 2007; Cusack et al., 2007) and LA-ICP-MS (Pérez-Huerta et al., 2008; Clark et al., 2016; Rollion-Bard et al., 2019). Therefore, these patterns indicate a strong positive association between the concentrations of Mg and S (Figs. 10–13), as also shown by England et al. (2007), Cusack et al. (2008a) and Gaspard et al. (2018). In contrast, concentrations of Sr on the other hand are not higher in Mg-enriched bands and correlations between Mg/Ca and Sr/Ca in LA-ICP-MS transects are weak.

In all specimens, the Mg-enriched bands terminate at external growth lines and effectively copy the curvature of internal growth lines (Figs. 11 and 12). They start in the primary layer at the location of the external growth lines and propagate obliquely at a low angle (relative to the external surface) towards the internal surface, converge and become almost parallel with the inner surface. When comparing EPMA transects with EPMA maps, these bands clearly coincide with the location of the major peaks in Mg/Ca in extant and extinct brachiopods (Figs. 10–12). Mg/Ca in Mg-enriched bands are two to four times higher than mean background values, often approaching values measured in the primary layer. The sharp maxima in Mg/Ca observed in longitudinal LA-ICP-MS transects thus correspond to the same peaks (Figs. 6–8). Therefore, even when spot size in the LA-ICP-MS measurements is less resolved (35 μm) than in microprobe analyses (8 μm), laser-ablation is able to detect the presence of thin bands and the magnitude of Mg/Ca maxima. The overall comparison of LA-ICP-MS and EPMA shows that Mg/Ca values in six equivalent transects are coeval and that these two methods give congruent and comparable results (Fig. 9).

4. Discussion

4.1. Association of Mg-enrichment with external growth lines

In accord with previous studies, high-resolution methods based on LA-ICP-MS and EPMA show that the major within-shell variation in Mg/Ca occurs between the Mg-rich primary layer and the Mg-poor secondary layer (Figs. 5 and 10–12) (England et al., 2007; Cusack et al., 2008a; Pérez-Huerta et al., 2008; Rollion-Bard et al., 2016). The primary layer is precipitated under a different secretion regime dominated by extracellular rather than intracellular precipitation, generating disordered

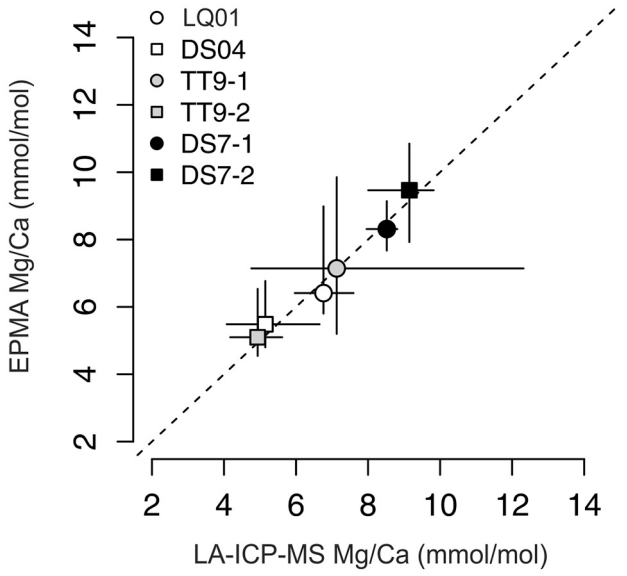

Fig. 9. The comparison of median Mg/Ca values for six, 2–3 mm-long transects based on LA-ICP-MS and EPMA analyses (these transects are not precisely equivalent in terms of their location through the secondary layer but are expected to capture comparable portions of valves). Minima and maxima correspond to the 25th and 75th percentiles of Mg/Ca distributions in each transect.

acicular calcite rather than fibrous calcite (Williams, 1968; Griesshaber et al., 2007). Two main types of Mg/Ca variation patterns were observed within the secondary layer, including (1) differences between anterior (not affected by resorption) and posterior portions of valves (that contain internal structures affected by resorption, such as loops, muscle scars, median septum), which can be also enriched in Mg (Rollion-Bard et al., 2016; Ullmann et al., 2017a), and (2) differences between background, relatively uniform levels of Mg/Ca and sharp on the one hand, and narrow, high-magnitude peaks in Mg/Ca terminating at external growth lines on the other hand. Notably, here Mg/Ca maxima, increasing by a factor of two to four above the background Mg/Ca values, can attain values comparable to those in the primary layer. We document this second pattern both in fossil (tropical) and Recent (temperate) terebratulid and rhynchonellid brachiopods, indicating that it is a general pattern that does not depend on some unique combination of temporal or environmental circumstances and applies equally to species with and without punctae. Although the relatively regular fluctuations in Mg/Ca within the secondary layer were linked to seawater temperature seasonality (Butler et al., 2015; Clark et al., 2016), however, the association of Mg/Ca maxima with external growth lines contradicts this hypothesis. We suggest that this pattern might reflect seasonal changes in shell growth rate (not necessarily to the growth rate of calcite, but rather to the rate of transformation of ACC to calcite, see below) and is not related to seasonally warmer seawater temperature that can increase Mg incorporation into the calcite lattice.

Although the timing of growth cessation for *N. nigricans* and *M. sanguinea* is not independently documented, cold-temperate brachiopods from New Zealand are active and spawn during the spring-

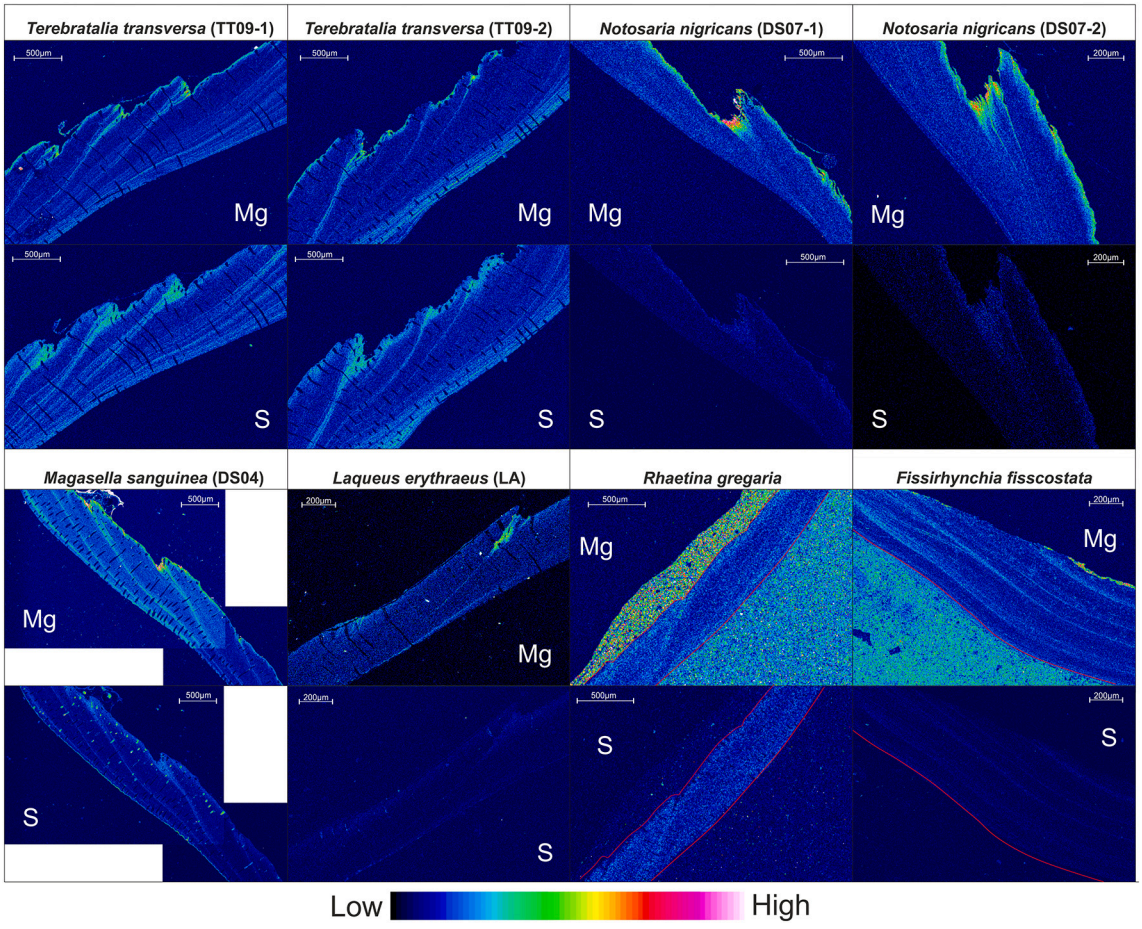

Fig. 10. EMPA maps showing Mg, S and Sr distribution in each of the studied specimens. Areas of lighter color are indicating high element concentration, while darker colors are marking areas with lower element concentration.

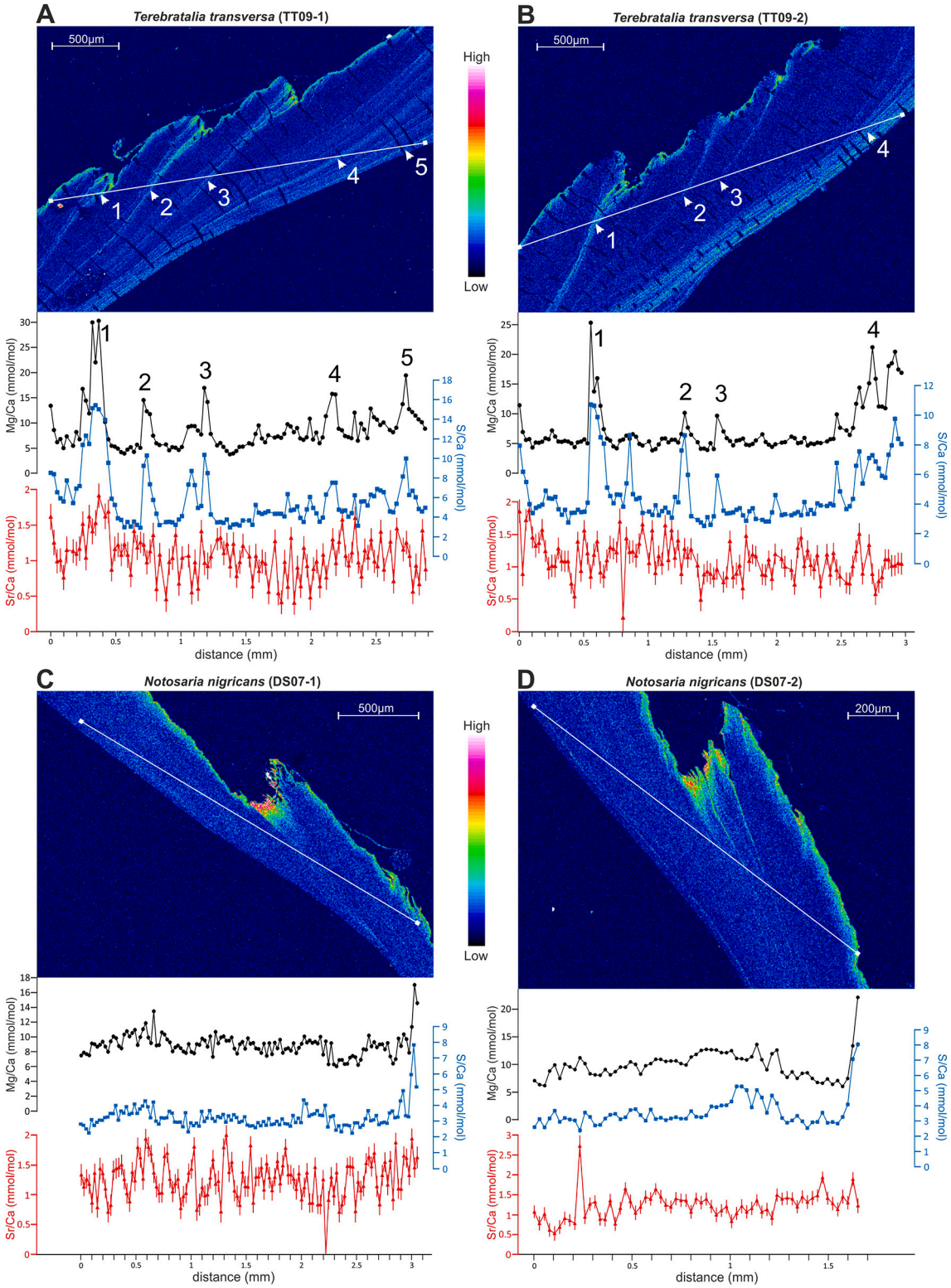

Fig. 11. EMPA maps of Mg distribution and Mg/Ca, S/Ca and Sr/Ca profiles of spot analyses of the specimens TT09 – *T. transversa* (A and B) and DS07 – *N. nigricans* (C and D). White lines indicate the area where microprobe sections were analyzed. Arrows and numbers are showing how the observed peaks in Mg/Ca along the sections are corresponding to the Mg enriched bands on the maps. Warmer colors on the color scale bars indicate higher Mg concentration.

autumn and their growth rate is slowest during the austral winter when the productivity is smallest (Rickwood, 1977), as is typical of cold-temperate benthic groups in general (Coma et al., 2000). In accord with this, external growth lines on cold-temperate populations of *T. transversa* from the San Juan Archipelago closely coincide with the most positive value of $\delta^{18}O$ (Auclair et al., 2003), indicating that the growth cessation in this brachiopod also occurs in winter when food is less available (Masson and Peña, 2009). The decline in Mg/Ca predicted to occur under reduced temperature is thus cancelled out by some other mechanism that induces Mg-enrichment occurring during winter in

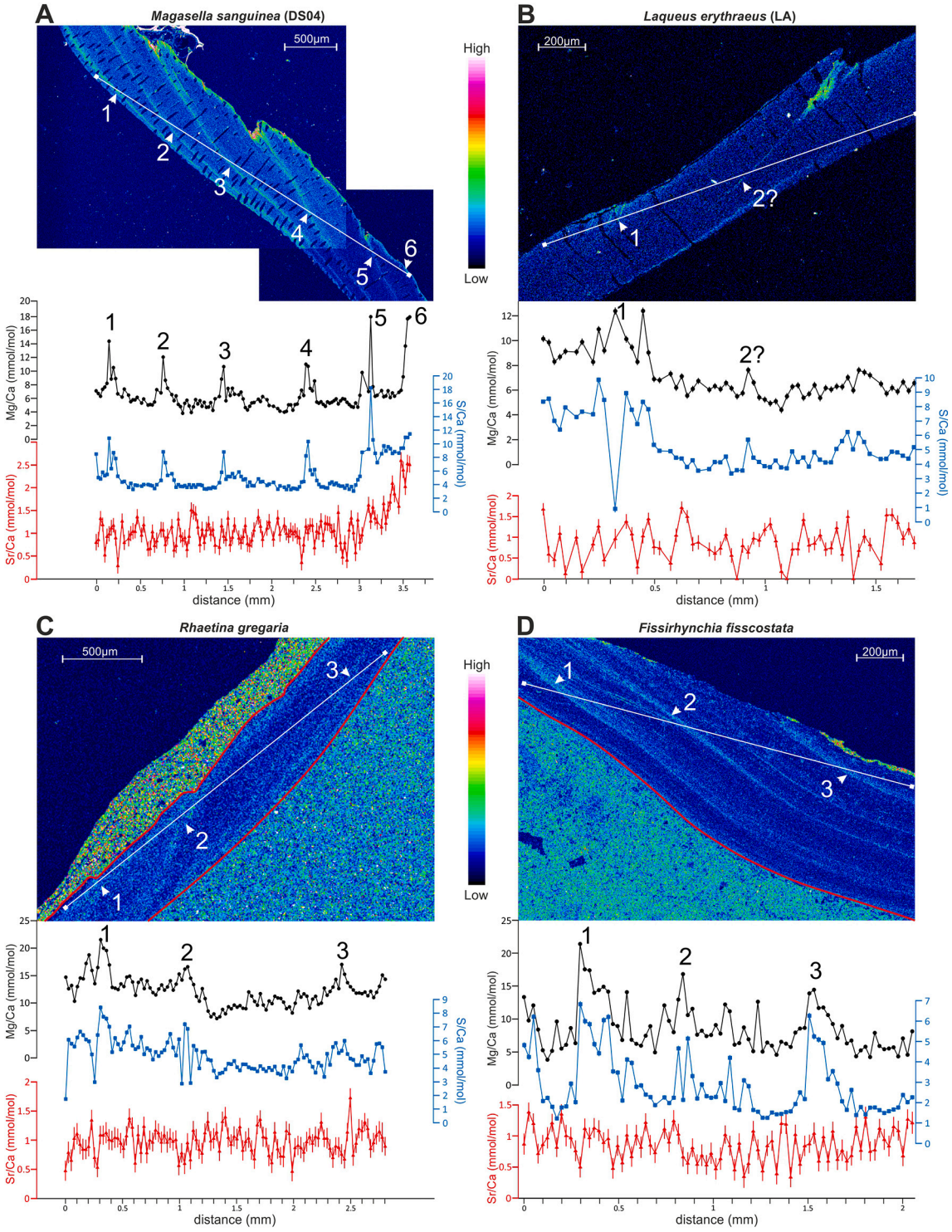

Fig. 12. EMPA maps of Mg distribution and Mg/Ca, S/Ca and Sr/Ca profiles of spot analyses of the specimens DS04 – *M. sanguinea* (A), LA – *L. erythraeus* (B), *R. gregaria* (C) and *F. fisscostata* (D). White lines indicate the area where microprobe sections were analyzed. Arrows and numbers are showing how the observed peaks in Mg/Ca along the sections are corresponding to the Mg enriched bands on the maps. Red lines are marking the sediment-shell boundary. Warmer colors on the color scale bars indicate higher Mg concentration. (For interpretation of the references to color in this figure legend, the reader is referred to the web version of this article.)

these cold-temperate brachiopods. However, we stress that the formation of growth lines in brachiopods or mollusks can be determined by various mechanisms and occur under various environmental stresses or disturbances (Hiller, 1988; Pérez-Huerta et al., 2013) and the growth cessation can also occur in summer in other marine invertebrate groups, especially in warm-temperate benthic taxa (Coma et al., 2000). Therefore, Mg-enriched bands observed in other studies of brachiopod shells may thus coincide with higher temperature seasons, depending on the seasonality of growth cessation. For example, the timing of formation of growth lines in fossil brachiopods analyzed here is not yet constrained.

Given that the magnitude of Mg/Ca in micrometric growth bands is comparable to values in the primary layers, exceeding background Mg/Ca minima by 5–10 mmol/mol or more (Figs. 11 and 12), and assuming that calibration of temperature by Mg/Ca is comparable to that of

calcitic bivalves (Vander Putten et al., 2000), such difference would indicate changes in seawater temperature significantly exceeding 5 °C, in contrast to the observed annual seawater temperature range at all locations (<5 °C). Regardless of the mechanisms triggering Mg-enrichment in brachiopod shells during the growth cessation, Mg/Ca values associated with growth lines should be excluded from inferences based on Mg/Ca paleothermometry.

In addition to changes in Mg/Ca related to changes in temperature, Mg/Ca variability can reflect changes in calcite precipitation rates. For example, higher Mg values can reflect higher growth rates in juvenile phase (so-called primary ontogenetic pattern in Mg concentrations in Buening and Carlson, 1992). Buening and Carlson (1992) observed that elevated (and variable) levels of Mg in the posteriormost, juvenile portions of valves, followed by lower, more stable Mg concentrations in anterior, ontogenetically older parts. Similarly, Butler et al. (2015) observed a ten-fold increase in Mg/Ca and a two-fold increase in Sr/Ca in the youngest part of *Terebratulina retusa* and *Liothyrella neozelanica*. These patterns appear to be related to a predictable decrease in growth rate through ontogeny, and thus seem to support the positive effect of precipitation rate on incorporation of Mg (Ullmann et al., 2017b). Indeed, three extant species studied here show an ontogenetic decline in growth rate. However, there is no corresponding change in Mg/Ca within the secondary layer. Mg-enrichment in both studies (Buening and Carlson, 1992; Butler et al., 2015) is rather associated with sharp and narrow peaks in Mg that are similar to those associated with growth lines in this study (and thus not with seasonal maxima in primary productivity as initially suggested for *T. transversa* by Buening and Carlson, 1992). We suggest the high variance in Mg/Ca observed in those studies thus does not reflect the overall decline in growth rate because (1) Mg-enrichment is associated with growth minima, not with growth maxima, and (2) Mg maxima in those studies seems to be rather driven by high variance of Mg in the posteriormost parts. We do not observe any consistent species-specific Mg/Ca or Sr/Ca trends related to ontogeny, and any trend is overwhelmed by Mg/Ca maxima that extend 5–10 mmol/mol above the background values.

4.2. The paradox of high Mg uptake under slow growth rate

Several studies show that an increase in the precipitation rate of inorganic calcite can increase Mg incorporation (Mavromatis et al., 2013, Goetschl et al., 2019; although this dependence is not straightforward, Mucci and Morse, 1983; Gabitov et al., 2014; Nürnberg et al., 1996) and the presence of organic ligands during inorganic calcite precipitation can also increase Mg incorporation (Wang et al., 2009; Mavromatis et al., 2017). The incorporation of sulfur into calcite is expected to increase with calcite growth rate (Busenberg and Plummer, 1985; Richardson et al., 2019). Therefore, our observation that Mg- and S-enrichments in the secondary layer at the location of growth lines is paradoxical. However, the association of Mg with growth lines is pervasive in not only our study, but also in other studies documenting brachiopods and calcitic or bimineralic bivalves (Dauphin et al., 2003; Gaspard et al., 2018; Tanaka et al., 2019; Jurikova et al., 2020). These findings indicate that the mechanism that leads to Mg enrichment in brachiopods at times of growth cessation can be related to the hypothesis of Rollion-Bard et al. (2019) that Mg is in fact incorporated into amorphous calcium carbonate (ACC) during initial phases of precipitation of calcium carbonate, prior to its crystallization to calcite. Our observation that the highest Mg/Ca values in the Mg-enriched bands in the secondary layer consistently coincide with the highest Mg/Ca values in the primary layer can support this hypothesis. Although, in vitro transformation of ACC to crystalline calcium carbonate proceeds via dissolution and reprecipitation (Wolf et al., 2008; Giuffre et al., 2015; Blue et al., 2017), most in vivo studies of biogenic carbonates revealed a solid-state process involving dehydration and structural re-arrangement (Politi et al., 2009; Weiner and Addadi, 2011). Additionally, combination of dissolution-reprecipitation and solid-state transformation processes may also exists, with the predominance of either being controlled by the crystallization fluid (Gal et al., 2014; Giuffre et al., 2015). If some solid-state transformation occurs during biomineralization of brachiopod shells, then it might also possible that the transformation of amorphous calcium carbonate (the potential precursor of calcitic fibers in brachiopods, Griesshaber et al., 2009; Cusack et al., 2010; Gaspard and Nouet, 2016; Rollion-Bard et al., 2019) to calcitic fibers is delayed or interrupted at times of stress, not by the inhibition of crystallization per se, but by limitation on protein formation (e.g., induced by low productivity or by thermal stress). As ACC needs to be stabilized by higher incorporation of Mg to retard crystal formation (Loste et al., 2003; Politi et al., 2009; Cartwright et al., 2012), and since ACC can be also more susceptible to incorporation of larger sulfate ions (Richardson et al., 2019), the delayed transformation of ACC to calcite can ultimately generate thin zones enriched with Mg and S that coincide with growth lines. For example, Pérez-Huerta et al. (2013) interpreted significant Mg-enrichment in growth lines in aragonitic bivalves as being driven by the incorporation of Mg by ACC when the heat stress inhibited the protein formation and the subsequent growth of crystals.

4.3. The role of organics

The mantle retraction can result in the deposition of organics on the inner side of the secondary layer in extant rhynchonelliformean brachiopods (Hiller, 1988), suggesting that S-enrichment might reflect sulphate in organic matter in these zones. However, S-enrichment does not seem to reflect sulphate in organic matter because sulfur in brachiopod shells is mostly situated in the calcite crystals and the intercrystalline organic matter has a negligible S concentration (Richardson et al., 2019). Our observations also support this inference for our brachiopod samples, because the high-resolution BSE images and elemental maps of an area of Mg and S enriched bands of *T. transversa* (Fig. 13) show that these Mg-enriched bands are not darker in BSE images, i.e., do not seem to be significantly enriched in (low-density) organic matter concentration relative to Mg-poor areas (e.g., England et al., 2007). In addition, the distribution of Mg in the Mg-enriched bands is not bound to between-fiber boundaries (where the majority of intra-shell organic matter is located) and a significant enrichment occurs within the calcite fibers (Fig. 13). Therefore, the observed fluctuation of Mg/Ca in the secondary layer of brachiopods analyzed here is not linked to variability in the concentration of organic matter and organics have a negligible effect on the concentration differences of Mg in the secondary layer.

4.4. Implications for the Mg/Ca as a paleothermometer in the fossil record

It seems paradoxical that many empirical studies found negative interspecific relation between Mg/Ca of the secondary layer and $\delta^{18}O$ of the corresponding shell part in fossil brachiopods (Mii and Grossman, 1994; Armendáriz et al., 2008). However, these correlations are typically based on coarser sampling resolution that spans several hundreds of micrometers. Such Mg/Ca values can reflect background values that correspond to a normal positive precipitation regime (when ACC quickly transformed to calcite fibers) and can be less affected by thin Mg-enriched bands. Therefore, we emphasize that long-term changes in average per-shell Mg/Ca values measured in the secondary layer of brachiopods can be still used in historical reconstructions of seawater temperature but the Mg/Ca maxima associated with external growth lines should be filtered out from such analyses. However, if fluctuations in Mg/Ca are associated with growth lines we suggest that care must be taken when Mg/Ca ratio in brachiopod shells is applied as a proxy of temperature or seasonality.

5. Conclusions

One of the major problems in assessing intra-shell variability in Mg/

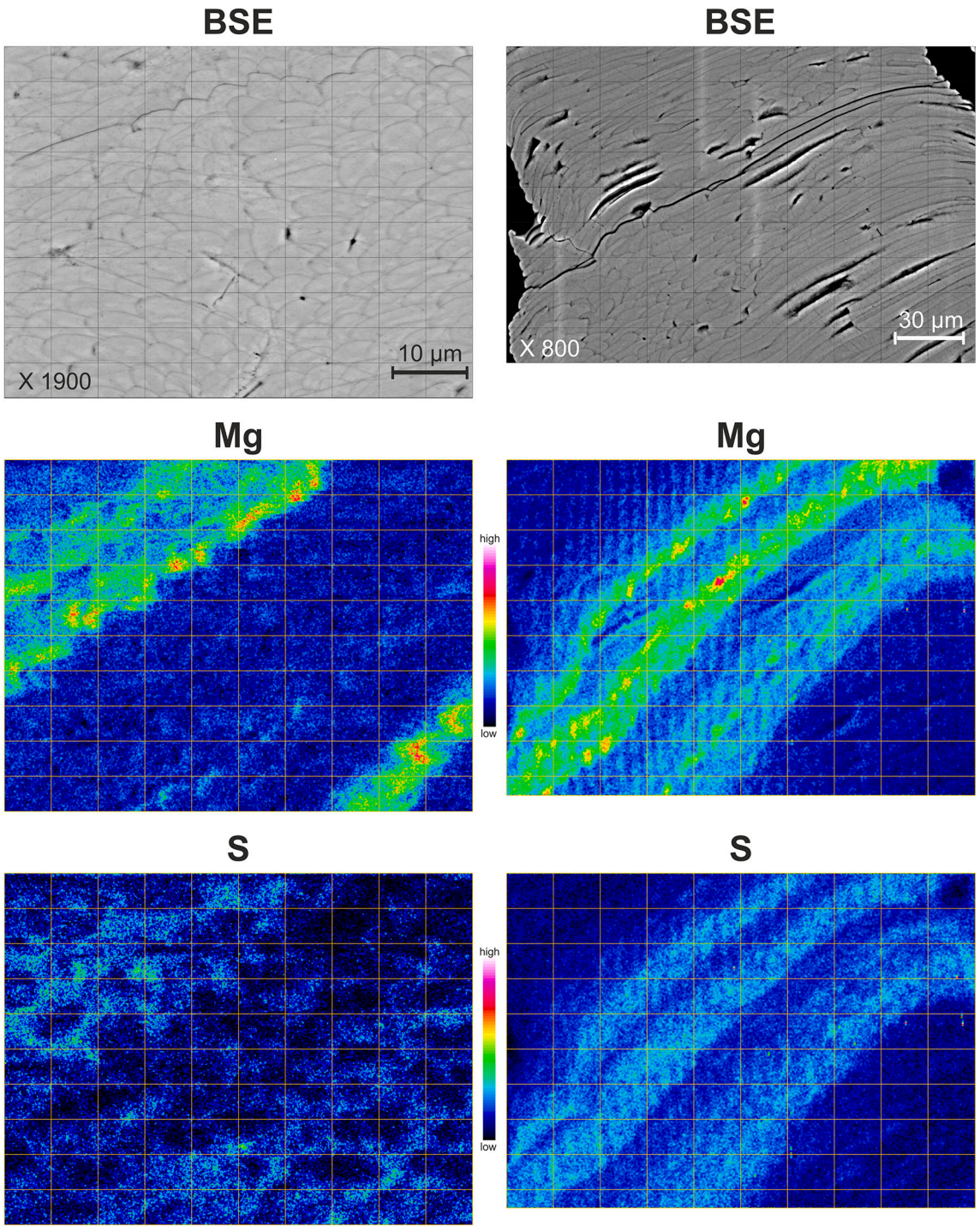

Fig. 13. BSE images and elemental maps of Mg, and S in Mg-enriched bands in anteriormost part of ventral valves of *Terebratalia transversa* (TT09). The BSE images show cross-sections of calcitic fibers and does not indicate any significant enrichment in low-density organic matter concertation that would be expected to generate darker zones at the location of Mg-enriched bands. The distribution pattern of elements indicates that the Mg and S enrichments affect the calcite fibers (and is not limited boundaries between fibers). The distribution pattern of S is more patchy, but overlaps with Mg. Color bars indicate relative element concentrations.

Ca is that peaks in Mg/Ca were rarely related to growth lines. Internal growth lines in brachiopod shells are not easily visible in translucent sections and mapping growth lines to wiggles in Mg/Ca on the basis of LA-ICP-MS or EPMA transects in the absence of spatial maps is thus difficult. The distribution of the trace elements Mg, S and Sr and their ratios to Ca (Mg/Ca, S/Ca and Sr/Ca), as evaluated by EPMA element maps and transect analyses and LA-ICP-MS on four extant brachiopod species (*T. transversa*, *N. nigricans, Magasella sanguinea* and *Laqueus erythraeus*) and two fossil species (*Rhaetina gregaria* and *Fissirhynchia fissicostata*), demonstrate that Mg enrichments in the secondary layer are induced by growth slowdown or cessation and not by direct effect of seawater temperature on Mg-incorporation into calcite.

We show that Mg/Ca maxima in the secondary layer of brachiopod shells are forming 10–50 µm wide bands that are clearly overlapping with growth lines on the external surface, revealing an internal growth structure. The spacing of external growth lines indicates that they are primarily representing annual cessations of growth. The examples of cold-temperate brachiopods that mainly form external growth lines in

winter (although growth cessation can also occur in summer in other benthic groups) shows potential decoupling in Mg/Ca and the role of temperature. Although the mechanisms that lead to Mg and S enrichment in the secondary shell layer at the location corresponding to growth cessation remain unclear, we suggest that this pattern can be explained by the Mg-stabilization of ACC so that the transformation into calcitic fibers is delayed or interrupted at times of environmental stress, ultimately generating thin zones enriched with Mg and S that coincide with growth lines.

Supplementary data to this article can be found online at https://doi.org/10.1016/j.chemgeo.2022.120758.

Declaration of Competing Interest

The authors declare that they have no known competing financial interests or personal relationships that could have appeared to influence the work reported in this paper.

Acknowledgments

We thank Dorrit E. Jacob (Macquarie University) for helping with part of the LA-ICP-MS analyses and J. Farkaš for discussions. This project was funded by the European Union's Horizon 2020 Research and Innovation Program under the Marie Skłodowska-Curie grant agreement and project BASE-LiNE Earth [No. 643084], by the Slovak Scientific Grant Agency (VEGA 0136/15) and by the Slovak Research and Development Agency (APVV 17-0555). This study received partial funding by the National Research, Development and Innovation Office of Hungary (grant OTKA K 135309). The research was also supported by the European Union and the State of Hungary, co-financed by the European Regional Development Fund in the project of GINOP-2.3.2.-15-2016-00009 'ICER'. The insights and comments from two anonymous reviewer helped to strengthen the final version of the manuscript and are gratefully acknowledged. This is CNR-ISMAR Bologna scientific contribution n. 1982.

References

Anand, P., Elderfield, H., Conte, M.H., 2003. Calibration of Mg/Ca thermometry in planktonic foraminifera from a sediment trap time series. Paleoceanography. 18 (2).
Armendáriz, M., Rosales, I., Quesada, C., 2008. Oxygen isotope and Mg/Ca composition of late Viséan (Mississippian) brachiopod shells from SW Iberia: palaeoclimatic and palaeogeographic implications in northern Gondwana. Palaeogeogr. Palaeoclimatol. Palaeoecol. 268, 65–79.
Auclair, A.C., Joachimski, M.M., Lécuyer, C., 2003. Deciphering kinetic, metabolic and environmental controls on stable isotope fractionations between seawater and the shell of *Terebratalia transversa* (Brachiopoda). Chem. Geol. 202 (1–2), 59–78.
Bajnai, D., Fiebig, J., Tomašových, A., Garcia, S.M., Rollion-Bard, C., Raddatz, J., Löffler, N., Primo-Ramos, C., Brand, U., 2018. Assessing kinetic fractionation in brachiopod calcite using clumped isotopes. Sci. Rep. 8, 533.
Barker, S., Cacho, I., Benway, H., Tachikawa, K., 2005. Planktonic foraminiferal Mg/Ca as a proxy for past oceanic temperatures: a methodological overview and data compilation for the last Glacial Maximum. Quat. Sci. Rev. 24 (7), 821–834.
Beck, W.J., Edwards, R.L., Ito, E., Taylor, F.W., Recy, J., Rougerie, F., Joannot, P., Henim, C., 1992. Sea-Surface temperature from coral skeletal strontium/calcium ratios. Science. 257, 644–664.
Berner, R.A., 1975. The role of magnesium in the crystal growth of calcite and aragonite from sea water. Geochim. Cosmochim. Acta 39 (4), 489–504.
Blue, C.R., Giuffre, A., Mergelsberg, S., Han, N., De Yoreo, J.J., Dove, P.M., 2017. Chemical and physical controls on the transformation of amorphous calcium carbonate into crystalline CaCO3 polymorphs. Geochim. Cosmochim. Acta 196, 179–196.
Brand, U., Logan, A., Hiller, N., Richardson, J., 2003. Geochemistry of modern brachiopods: applications and implications for oceanography and paleoceanography. Chem. Geol. 198 (3–4), 305–334.
Brand, U., Azmy, K., Bitner, M.A., Logan, A., Zuschin, M., Came, R., Ruggiero, E., 2013. Oxygen isotopes and $MgCO_3$ in brachiopod calcite and a new paleotemperature equation. Chem. Geol. 359, 23–31.
Brey, T., Peck, L.S., Gutt, J., Hain, S., Arntz, W.E., 1995. Population dynamics of *Magellania fragilis*, a brachiopod dominating a mixed-bottom macrobenthic assemblage on the Antarctic shelf. J. Mar. Biol. Assoc. U. K. 75 (4), 857–869.
Broecker, W., Yu, J., 2011. What do we know about the evolution of Mg to ca ratios in seawater? Paleoceanography. 26, PA3203.
Buening, N., Carlson, S.J., 1992. Geochemical investigation of growth in selected recent articulate brachiopods. Lethaia. 25, 331–345.
Busenberg, E., Plummer, L.N., 1985. Kinetic and thermodynamic factors controlling the distribution of SO_4^{2-} and Na^+ in calcites and selected aragonites. Geochim. Cosmochim. Acta 49, 713–725.
Butler, S., Bailey, T.R., Lear, C.H., Curry, G.B., Cherns, L., McDonald, I., 2015. The Mg/Ca–temperature relationship in brachiopod shells: calibrating a potential palaeoseasonality proxy. Chem. Geol. 397, 106–117.
Carpenter, S.J., Lohmann, K.C., 1992. Sr/Mg ratios of modern marine calcite: Empirical indicators of ocean chemistry and precipitation rate. Geochim. Cosmochim. Acta 56, 1837–1849.
Carpenter, S.J., Lohmann, K.C., 1995. $\delta^{18}O$ and $\delta^{13}C$ values of modern brachiopod shells. Geochim. Cosmochim. Acta 59 (18), 3749–3764.
Cartwright, J.H., Checa, A.G., Gale, J.D., Gebauer, D., Sainz-Díaz, C.I., 2012. Calcium carbonate polyamorphism and its role in biomineralization: how many amorphous calcium carbonates are there? Angew. Chem. Int. Ed. 51 (48), 11960–11970.
Clark, J.V., Pérez-Huerta, A., Gillikin, D.P., Aldridge, A.E., Reolid, M., Endo, K., 2016. Determination of paleoseasonality of fossil brachiopods using shell spiral deviations and chemical proxies. Palaeoworld. 25 (4), 662–674.
Coma, R., Ribes, M., Gili, J.-M., Zabala, M., 2000. Seasonality in coastal benthic ecosystems. Trends Ecol. Evol. 15 (11), 448–453.
Cusack, M., Parkinson, D., Pérez-Huerta, A., England, J., Curry, G.B., Fallick, A.E., 2007. Relationship between $\delta^{18}O$ and minor element composition of *Terebratalia transversa*. Earth Environ. Sci. Trans. Royal Soc. Edinburgh. 98 (3–4), 443–449.
Cusack, M., Dauphin, Y., Cuif, J.P., Salomé, M., Freer, A., Yin, H., 2008a. Micro-XANES mapping of Sulphur and its association with magnesium and phosphorus in the shell of the brachiopod, *Terebratulina retusa*. Chem. Geol. 253 (3–4), 172–179.
Cusack, M., Pérez-Huerta, A., Janousch, M., Finch, A.A., 2008b. Magnesium in the lattice of calcite-shelled brachiopods. Chem. Geol. 257 (1–2), 59–64.
Cusack, M., Chung, P., Dauphin, Y., Pérez-Huerta, A., 2010. Brachiopod primary layer crystallography and nanostructure. Spec. Pap. Palaeontol. 84, 99–105.
Dauphin, Y., Cuif, J., Doucet, J., Salomé, M., Susini, J., Williams, C., 2003. In situ mapping of growth lines in the calcitic prismatic layers of mollusc shells using X-ray absorption near-edge structure (XANES) spectroscopy at the Sulphur K-edge. Mar. Biol. 142 (2), 299–304.
Davis, K.J., Dove, P.M., De Yoreo, J.J., 2000. The role of Mg^{2+} as an impurity in calcite growth. Science. 290 (5494), 1134–1137.
Dickson, J.A.D., 2002. Fossil echinoderms as monitor of the Mg/ca ratio of Phanerozoic oceans. Science. 298 (5596), 1222–1224.
England, J., Cusack, M., Lee, M.R., 2007. Magnesium and sulphur in the calcite shells of two brachiopods, *Terebratulina retusa* and *Novocrania anomala*. Lethaia. 40 (1), 2–10.
Gabitov, R.I., Sadekov, A., Leinweber, A., 2014. Crystal growth rate effect on Mg/Ca and Sr/Ca partitioning between calcite and fluid: an in situ approach. Chem. Geol. 367, 70–82.
Gal, A., Kahil, K., Vidavsky, N., DeVol, R.T., Gilbert, P.U.P.A., Fratzl, P., Weiner, S., Addadi, L., 2014. Particle accretion mechanism underlies biological crystal growth from an amorphous precursor phase. Adv. Funct. Mater. 24, 5420–5426.
Gaspard, D., Nouet, J., 2016. Hierarchical architecture of the inner layers of selected extant rhynchonelliform brachiopods. J. Struct. Biol. 196 (2), 197–205.
Gaspard, D., Aldridge, A.E., Boudouma, O., Fialin, M., Rividi, N., Lécuyer, C., 2018. Analysis of growth and form in *Aerothyris kerguelenensis* (rhynchonelliform brachiopod)-Shell spiral deviations, microstructure, trace element contents and stable isotope ratios. Chem. Geol. 483, 474–490.
Giuffre, A.J., Gagnon, A.C., De Yoreo, J.J., Dove, P.M., 2015. Isotopic tracer evidence for the amorphous calcium carbonate to calcite transformation by dissolution–reprecipitation. Geochim. Cosmochim. Acta 165, 407–417.
Goetschl, K.E., Purgstaller, B., Dietzel, M., Mavromatis, V., 2019. Effect of sulfate on magnesium incorporation in low-magnesium calcite. Geochim. Cosmochim. Acta 265, 505–519.
Griesshaber, E., Schmahl, W.W., Neuser, R., Pettke, T., Blüm, M., Mutterlose, J., Brand, U., 2007. Crystallographic texture and microstructure of terebratulide brachiopod shell calcite: an optimized materials design with hierarchical architecture. Am. Mineral. 92 (5–6), 722–734.
Griesshaber, E., Kelm, K., Sehrbrock, A., Mader, W., Mutterlose, J., Brand, U., Schmahl, W.W., 2009. Amorphous calcium carbonate in the shell material of the brachiopod *Megerlia truncata*. Eur. J. Mineral. 21 (4), 715–723.
Grossman, E.L., Mii, H.S., Yancey, T.E., 1993. Stable isotopes in late Pennsylvanian brachiopods from the United States: Implications for Carboniferous paleoceanography. Geol. Soc. Am. Bull. 105 (10), 1284–1296.
Grossman, E.L., Mii, H.S., Zhang, C., Yancey, T.E., 1996. Chemical variation in Pennsylvanian brachiopod shells; diagenetic, taxonomic, microstructural, and seasonal effects. J. Sediment. Res. 66 (5), 1011–1022.
Henkes, G.A., Passey, B.H., Wanamaker Jr., A.D., Grossman, E.L., Ambrose Jr., W.G., Carroll, M.L., 2013. Carbonate clumped isotope compositions of modern marine mollusk and brachiopod shells. Geochim. Cosmochim. Acta 106, 307–325.
Hiller, N., 1988. The development of growth lines on articulate brachiopods. Lethaia. 21, 177–188.
Immenhauser, A., Nägler, T.F., Steuber, T., Hippler, D., 2005. A critical assessment of mollusk $^{18}O/^{16}O$, Mg/Ca, and $^{44}Ca/^{40}Ca$ ratios as proxies for cretaceous seawater temperature seasonality. Palaeogeogr. Palaeoclimatol. Palaeoecol. 215 (3–4), 221–237.
Jochum, K.P., Nohl, U., Herwig, K., Lammel, E., Stoll, B., Hofmann, A.W., 2005. GeoReM: a new geochemical database for reference materials and isotopic standards. Geostand. Geoanal. Res. 29 (3), 333–338.
Jochum, K.P., Weis, U., Stoll, B., Kuzmin, D., Yang, Q., Raczek, I., Jacob, D.E., Stracke, A., Birbaum, K., Frick, D.A., Günther, D., Enzweiler, J., 2011. Determination

of reference values for NIST SRM 610-617 glasses following ISO guidelines. Geostand. Geoanal. Res. 35, 397–429. https://doi.org/10.1111/j.1751-908X.2011.00120.x.
Jurikova, H., Ippach, M., Liebetrau, V., Gutjahr, M., Krause, S., Büsse, S., Gorb, S.N., Henkel, D., Hiebenthal, C., Schmidt, M., Leipe, T., 2020. Incorporation of minor and trace elements into cultured brachiopods: implications for proxy application with new insights from a biomineralisation model. Geochim. Cosmochim. Acta 286, 418–440.
Klein, R.T., Lohmann, K.C., Thayer, C.W., 1996. Bivalve skeletons record sea-surface temperature and $\delta^{18}O$ via Mg/Ca and $^{18}O/^{16}O$ ratios. Geology. 24 (5), 415–418.
Kocsis, L., Dulai, A., Cipriani, A., Vennemann, T., Yunsi, M., 2020. Geochemistry of recent and fossil brachiopod calcite of Megathiris detruncata (Terebratulida, Megathyrididae): a modern baseline study to trace past environmental conditions. Chem. Geol. 533, 119335.
Korte, C., Jasper, T., Kozur, H.W., Veizer, J., 2005. $\delta^{18}O$ and $\delta^{13}C$ of Permian brachiopods: a record of seawater evolution and continental glaciation. Palaeogeogr. Palaeoclimatol. Palaeoecol. 224 (4), 333–351.
Lamare, M.D., Stewart, B.G., 1998. Mass spawning by the sea urchin Evechinus chloroticus (Echinodermata: Echinoidea) in a New Zealand fiord. Mar. Biol. 132 (1), 135–140.
Lea, D.W., Mashiotta, T.A., Spero, H.J., 1999. Controls on magnesium and strontium uptake in planktonic foraminifera determined by live culturing. Geochim. Cosmochim. Acta 63 (16), 2369–2379.
Lear, C.H., Elderfield, H., Wilson, P.A., 2000. Cenozoic deep-sea temperatures and global ice volumes from Mg/Ca in benthic foraminiferal calcite. Science. 287 (5451), 269–272.
Lee, D.E., Robinson, J.H., Witman, J.D., Copeland, S.E., Harper, E.M., Smith, F., Lamare, M., 2011. Observations on recruitment, growth and ecology in a diverse living brachiopod community, doubtful sound, Fiordland, New Zealand. Spec. Pap. Palaeontol. 84, 177–191.
Longerich, H.P., Jackson, S.E., Günther, D., 1996. Inter-laboratory note. Laser ablation inductively coupled plasma mass spectrometric transient signal data acquisition and analyte concentration calculation. J. Anal. At. Spectrom. 11 (9), 899–904.
Loste, E., Wilson, R.M., Seshadri, R., Meldrum, F.C., 2003. The role of magnesium in stabilising amorphous calcium carbonate and controlling calcite morphologies. J. Cryst. Growth 254 (1–2), 206–218.
Lowenstam, H.A., 1961. Mineralogy, O^{18}/O^{16} ratios, and strontium and magnesium contents of recent and fossil brachiopods and their bearing on the history of the oceans. J. Geol. 69, 241–260.
Martin, P.A., Lea, D.W., Rosenthal, Y., Shackleton, N.J., Sarnthein, M., Papenfuss, T., 2002. Quaternary deep sea temperature histories derived from benthic foraminiferal Mg/Ca. Earth Planet. Sci. Lett. 198 (1–2), 193–209.
Masson, D., Peña, A., 2009. Chlorophyll distribution in a temperate estuary: the Strait of Georgia and Juan de Fuca Strait. Estuar. Coast. Shelf Sci. 82 (1), 19–28.
Mavromatis, V., Gautier, Q., Bosc, O., Schott, J., 2013. Kinetics of Mg partition and Mg stable isotope fractionation during its incorporation in calcite. Geochim. Cosmochim. Acta 114, 188–203. https://doi.org/10.1016/j.gca.2013.03.024.
Mavromatis, V., Immenhauser, A., Buhl, D., Purgstaller, B., Baldermann, A., Dietzel, M., 2017. Effect of organic ligands on Mg partitioning and Mg isotope fractionation during low-temperature precipitation of calcite in the absence of growth rate effects. Geochim. Cosmochim. Acta 207, 139–153. https://doi.org/10.1016/j.gca.2017.03.020.
Michalík, J., 1973. New information on the character of the Rhaetian at the locality near Hybe (northern slope of the Tatry Mts., Slovakia). Geologické Práce Správy. 60, 197–212.
Mii, H.S., Grossman, E.L., 1994. Late Pennsylvanian seasonality reflected in the ^{18}O and elemental composition of a brachiopod shell. Geology. 22, 661–664.
Mucci, A., Morse, J.W., 1983. The incorporation of Mg2+ and Sr2+ into calcite overgrowths: influences of growth rate and solution composition. Geochim. Cosmochim. Acta 47, 217–233.
Nelson, G.A., 2014. Fishmethods: fishery science methods and models in R. In: R Package Version 1.7–0.
Novack-Gottshall, P.M., Lanier, M.A., 2008. Scale-dependence of Cope's rule in body size evolution of Paleozoic brachiopods. Proc. Natl. Acad. Sci. 105, 5430–5434.
Nunn, E.V., Price, G.D., 2010. Late Jurassic (Kimmeridgian–Tithonian) stable isotopes ($\delta^{18}O$, $\delta^{13}C$) and Mg/ca ratios: new palaeoclimate data from Helmsdale, Northeast Scotland. Palaeogeogr. Palaeoclimatol. Palaeoecol. 292, 325–335.
Nürnberg, D., Bijma, J., Hemleben, C., 1996. Assessing the reliability of magnesium in foraminiferal calcite as a proxy for water mass temperatures. Geochim. Cosmochim. Acta 60, 2483.
Ostrow, D.G., 2004. Larval Dispersal and Population Genetic Structure of Brachiopods in the New Zealand Fiords (Doctoral dissertation. University of Otago.
Parkinson, D., Curry, G.B., Cusack, M., Fallick, A.E., 2005. Shell structure, patterns and trends of oxygen and carbon stable isotopes in modern brachiopod shells. Chem. Geol. 219 (1–4), 193–235.
Pérez-Huerta, A., Cusack, M., Jeffries, T.E., Williams, C.T., 2008. High resolution distribution of magnesium and strontium and the evaluation of Mg/Ca thermometry in recent brachiopod shells. Chem. Geol. 247 (1–2), 229–241.
Pérez-Huerta, A., Etayo-Cadavid, M.F., Andrus, C.F.T., Jeffries, T.E., Watkins, C., Street, S.C., Sandweiss, D.H., 2013. El Niño impact on mollusk biomineralization–implications for trace element proxy reconstructions and the Paleo-archeological record. PLoS One 8 (2), 54274.
Politi, Y., Batchelor, D.R., Zaslansky, P., Chmelka, B.F., Weaver, J.C., Sagi, I., Weiner, S., Addadi, L., 2009. Role of magnesium ion in the stabilization of biogenic amorphous calcium carbonate: a structure–function investigation. Chem. Mater. 22, 161–166.
Popp, B.N., Podosek, F.A., Brannon, J.C., Anderson, T.F., Pier, J., 1986. $^{87}Sr/^{86}Sr$ ratios in Permo-Carboniferous Sea water from the analyses of well-preserved brachiopod shells. Geochim. Cosmochim. Acta 50 (7), 1321–1328.
Poulain, C., Gillikin, D.P., Thébault, J., Munaron, J.M., Bohn, M., Robert, R., Paulet, Y. M., Lorrain, A., 2015. An evaluation of Mg/Ca, Sr/Ca, and Ba/ca ratios as environmental proxies in aragonite bivalve shells. Chem. Geol. 396, 42–50.
Powell, M.G., Schöne, B.R., Jacob, D.E., 2009. Tropical marine climate during the late Paleozoic ice age using trace element analyses of brachiopods. Palaeogeogr. Palaeoclimatol. Palaeoecol. 280 (1–2), 143–149.
Price, G.D., Twitchett, R.J., Wheeley, J.R., Buono, G., 2013. Isotopic evidence for long term warmth in the Mesozoic. Sci. Rep. 3, 1438.
Richardson, J.A., Newville, M., Lanzirotti, A., Webb, S.M., Rose, C.V., Catalano, J.G., Fike, D.A., 2019. The source of sulfate in brachiopod calcite: insights from μ-XRF imaging and XANES spectroscopy. Chem. Geol. 529, 119328.
Rickwood, A.E., 1977. Age, growth and shape of the intertidal brachiopod Waltonia inconspicua Sowerby, from New Zealand. Am. Zool. 17 (1), 63–73.
Ries, J.B., 2004. Effect of ambient Mg/Ca ratio on Mg fractionation in calcareous marine invertebrates: a record of the oceanic Mg/Ca ratio over the Phanerozoic. Geology. 32 (11), 981–984.
Ries, J.B., 2010. Geological and experimental evidence for secular variation in seawater Mg/Ca (calcite-aragonite seas) and its effects on marine biological calcification. Biogeosciences. 7, 2795–2849.
Roda, M.S., Griesshaber, E., Ziegler, A., Rupp, U., Yin, X., Henkel, D., Haussermann, V., Laudien, J., Brand, U., Eisenhauer, A., Checa, A.G., Schmahl, W.W., 2019a. Calcite fibre formation in modern brachiopod shells. Sci. Rep. 9, 598.
Roda, M.S., Ziegler, A., Griesshaber, E., Yin, X., Rupp, U., Greiner, M., Henkel, D., Häussermann, V., Eisenhauer, A., Laudien, J., Schmahl, W.W., 2019b. Terebratulide brachiopod shell biomineralization by mantle epithelial cells. J. Struct. Biol. 207 (2), 136–157.
Rollion-Bard, C., Saulnier, S., Vigier, N., Schumacher, A., Chaussidon, M., Lécuyer, C., 2016. Variability in magnesium, carbon and oxygen isotope compositions of brachiopod shells: Implications for paleoceanographic studies. Chem. Geol. 423, 49–60.
Rollion-Bard, C., Garcia, S.M., Burckel, P., Angiolini, L., Jurikova, H., Tomašových, A., Henkel, D., 2019. Assessing the biomineralization processes in the shell layers of modern brachiopods from oxygen isotopic composition and elemental ratios: Implications for their use as paleoenvironmental proxies. Chem. Geol. 524, 49–66.
Rosenthal, Y., Boyle, E.A., Slowey, N., 1997. Temperature control on the incorporation of magnesium, strontium, fluorine, and cadmium into benthic foraminiferal shells from Little Bahama Bank: prospects for thermocline paleoceanography. Geochim. Cosmochim. Acta 61 (17), 3633–3643.
Schöne, B.R., Zhang, Z., Jacob, D., Gillikin, D.P., Tütken, T., Garbe-Schönberg, D., McConnaughey, T., Soldati, A., 2010. Effect of organic matrices on the determination of the trace element chemistry (Mg, Sr, Mg/Ca, Sr/Ca) of aragonitic bivalve shells (*Arctica islandica*) — Comparison of ICP-OES and LA-ICP-MS data. Geochem. J. 44, 23–37.
Schöne, B.R., Zhang, Z., Radermacher, P., Thébault, J., Jacob, D.E., Nunn, E.V., Maurer, A.F., 2011. Sr/ca and Mg/Ca ratios of ontogenetically old, long-lived bivalve shells (*Arctica islandica*) and their function as paleotemperature proxies. Palaeogeogr. Palaeoclimatol. Palaeoecol. 302, 52–64.
Spalding, M.D., Fox, H.E., Allen, G.R., Davidson, N., Ferdaña, Z.A., Finlayson, M.A.X., Halpern, B.S., Jorge, M.A., Lombana, A.L., Lourie, S.A., Martin, K.D., 2007. Marine ecoregions of the world: a bioregionalization of coastal and shelf areas. BioScience. 57 (7), 573–583.
Steuber, T., Rauch, M., 2005. Evolution of the Mg/Ca ratio of cretaceous seawater: implications from the composition of biological low-Mg calcite. Mar. Geol. 217, 199–213.
Stull, J.K., Allen, M.J., Moore, S.L., Tang, C.L., 1999. Relative abundance and health of megabenthic invertebrate species on the southern California shelf in 1994. In: Southern California Coastal Water Research Project Annual Report, 2000, pp. 189–209.
Suan, G., Mattioli, E., Pittet, B., Lécuyer, C., Suchéras-Marx, B., Duarte, L.V., Philippe, M., Reggiani, L., Martineau, F., 2010. Secular environmental precursors to early Toarcian (Jurassic) extreme climate changes. Earth Planet. Sci. Lett. 290, 448–458.
Tanaka, K., Okaniwa, N., Miyaji, T., Murakami-Sugihara, N., Zhao, L., Tanabe, K., Schöne, B.R., Shirai, K., 2019. Microscale magnesium distribution in shell of Mediterranean mussel *Mytilus galloprovincialis*: an example of multiple factors controlling Mg/Ca in biogenic calcite. Chem. Geol. 511, 521–523.
Thayer, C.W., 1977. Recruitment, growth, and mortality of a living articulate brachiopod, with implications for the interpretation of survivorship curves. Paleobiology. 3, 98–109.
Tomašových, A., 2004. Microfacies and depositional environment of an Upper Triassic intra-platform carbonate basin: the Fatric Unit of the West Carpathians (Slovakia). Facies. 50, 77–105.
Tomašových, A., 2008. Substrate exploitation and resistance to biotic disturbance in the brachiopod *Terebratalia transversa* and the bivalve *Pododesmus macrochisma*. Mar. Ecol. Prog. Ser. 363, 157–170.
Tomašových, A., Farkaš, J., 2005. Cathodoluminescence of late Triassic terebratulid brachiopods: implications for growth patterns. Palaeogeogr. Palaeoclimatol. Palaeoecol. 216, 215–233.
Ullmann, C.V., Korte, C., 2015. Diagenetic alteration in low-Mg calcite from macrofossils: a review. Geol. Quart. 59 (1), 3–20.
Ullmann, C.V., Pogge von Strandmann, P.A., 2017. The effect of shell secretion rate on Mg/Ca and Sr/ca ratios in biogenic calcite as observed in a belemnite rostrum. Biogeosciences. 14, 89–97.

Ullmann, C.V., Böhm, F., Rickaby, R.E., Wiechert, U., Korte, C., 2013. The Giant Pacific Oyster (*Crassostrea gigas*) as a modern analog for fossil ostreoids: isotopic (Ca, O, C) and elemental (Mg/Ca, Sr/Ca, Mn/Ca) proxies. Geochem. Geophys. Geosyst. 14 (10), 4109–4120.

Ullmann, C.V., Frei, R., Korte, C., Lüter, C., 2017a. Element/Ca, C and O isotope ratios in modern brachiopods: Species-specific signals of biomineralization. Chem. Geol. 460, 15–24.

Ullmann, C.V., Korte, C., Bitner, M.A., Azmy, K., Brand, U., 2017b. Geochemistry of the brachiopod *Hemithiris psittacea* from the Canadian Arctic: Implications for high latitude palaeoclimate studies. Chem. Geol. 466, 187–198.

Vander Putten, E., Dehairs, F., Keppens, E., Baeyens, W., 2000. High resolution distribution of trace elements in the calcite shell layer of modern *Mytilus edulis*: environmental and biological controls. Geochim. Cosmochim. Acta 64 (6), 997–1011.

Veizer, J., Ala, D., Azmy, K., Bruckschen, P., Buhl, D., Bruhn, F., Carden, A.F.G., Diener, A., Ebneth, S., Godderis, Y., Jasper, T., Korte, C., Pawellek, F., Podlaha, G.O., Strauss, H., 1999. $^{87}Sr/^{86}Sr$, $\delta^{13}C$ and $\delta^{18}O$ evolution of Phanerozoic seawater. Chem. Geol. 161 (1–3), 59–88.

Wang, D., Wallace, A.F., De Yoreo, J.J., Dove, P.M., 2009. Carboxylated molecules regulate magnesium content of amorphous calcium carbonates during calcification. Proc. Natl. Acad. Sci. 106, 21511–21516.

Watanabe, T., Winter, A., Oba, T., 2001. Seasonal changes in sea surface temperature and salinity during the Little Ice Age in the Caribbean Sea deduced from Mg/Ca and $^{18}O/^{16}O$ ratios in corals. Mar. Geol. 173 (1–4), 21–35.

Weiner, S., Addadi, L., 2011. Crystallization pathways in biomineralization. Annu. Rev. Mater. Res. 41, 21–40.

Williams, A., 1968. Evolution of the shell structure of articulate brachiopods. Spec. Pap. Palaeontol. 2, 1–55.

Wolf, S.E., Leiterer, J., Kappl, M., Emmerling, F., Tremel, W., 2008. Early homogenous amorphous precursor stages of calcium carbonate and subsequent crystal growth in levitated droplets. J. Am. Chem. Soc. 130, 12342–12347.

Yamamoto, K., Asami, R., Iryu, Y., 2010. Carbon and oxygen isotopic compositions of modern brachiopod shells from a warm-temperate shelf environment, Sagami Bay, Central Japan. Palaeogeogr. Palaeoclimatol. Palaeoecol. 291 (3–4), 348–359.

Zhang, Z., Augustin, M., Payne, J.L., 2015. Phanerozoic trends in brachiopod body size from synoptic data. Paleobiology. 41 (3), 491–501.